PFC/JA-85-2

LONG-TIME QUASILINEAR EVOLUTION OF THE FREE ELECTRON LASER INSTABILITY FOR A RELATIVISTIC ELECTRON BEAM PROPAGATING THROUGH A HELICAL MAGNETIC WIGGLER

Ronald C. Davidson
Yuan-Zhao Yin

Plasma Fusion Center
Massachusetts Institute of Technology
Cambridge, Massachusetts 02139 USA

January 1985

LONG-TIME QUASILINEAR EVOLUTION OF THE FREE ELECTRON LASER INSTABILITY FOR A RELATIVISTIC ELECTRON BEAM PROPAGATING THROUGH A HELICAL MAGNETIC WIGGLER

Ronald C. Davidson†
Science Applications International Corporation, Boulder, Colorado, 80302
Yuan-Zhao Yin††
Plasma Fusion Center
Massachusetts Institute of Technology, Cambridge, Mass., 02139

ABSTRACT

The long-time quasilinear development of the free electron laser instability is investigated for a tenuous electron beam propagating in the z-direction through a helical wiggler field $\underset{\sim}{B}_0 = -\hat{B} \cos k_0 z\, \hat{e}_x - \hat{B} \sin k_0 z\, \hat{e}_y$. The analysis neglects longitudinal perturbations ($\delta\phi \simeq 0$) and is based on the nonlinear Vlasov-Maxwell equations for the class of beam distributions of the form $f_b(z,\underset{\sim}{p},t) = n_0 \delta(P_x)\delta(P_y) \times G(z,p_z,t)$, assuming $\partial/\partial x = 0 = \partial/\partial y$. The long-time quasilinear evolution of the system is investigated within the context of a simple "water-bag" model in which the average distribution function $G_0(p_z,t) = (2L)^{-1} \int_{-L}^{L} dz\, G(z,p_z,t)$ is assumed to have the rectangular form $G_0(p_z,t) = [2\Delta(t)]^{-1}$ for $|p_z - p_0(t)| \leq \Delta(t)$, and $G_0(p_z,t) = 0$ for $|p_z - p_0(t)| > \Delta(t)$. Making use of the quasilinear kinetic equations, a coupled system of nonlinear equations is derived which describes the self-consistent evolution of the mean electron momentum $p_0(t)$, the momentum spread $\Delta(t)$, the amplifying wave spectrum $|H_k(t)|^2$, and the complex oscillation frequency $\omega_k(t) + i\gamma_k(t)$. These coupled equations are solved numerically for a wide range of system parameters, assuming that the input power spectrum $P_k(t=0)$ is flat and non-zero for a finite range of wavenumber k that overlaps with the region of k-space where the initial growth rate satisfies $\gamma_k(t=0) > 0$. To summarize the qualitative features of the quasilinear evolution, as the wave spectrum amplifies it is found that there is a concommitant decrease in the mean electron energy $\gamma_0(t)mc^2 = [m^2c^4 + e^2\hat{B}^2/k_0 + p_0^2(t)c^2]^{\frac{1}{2}}$, an increase in the momentum spread $\Delta(t)$, and a downshift of the growth rate $\gamma_k(t)$ to lower k-values. After sufficient time has elapsed, the growth rate γ_k has downshifted sufficiently far in k-space that the region where $\gamma_k > 0$ no longer overlaps the region where the initial power spectrum $P_k(t=0)$ is non-zero. Therefore, the wave spectrum saturates, and $\gamma_0(t)$ and $\Delta(t)$ approach their asymptotic values.

---

†Permanent address: Plasma Fusion Center, Massachusetts Institute of Technology, Cambridge, Mass., 02139
††Permanent address: Institute of Electron Physics, Academia Sinica, Beijing People's Republic of China

1. INTRODUCTION AND SUMMARY

There is a growing theoretical[1-27] and experimental[30-40] evidence that free electron lasers[28,29] are effective sources for coherent radiation generation. Recent theoretical studies include investigations of nonlinear effects[1-9] and saturation mechanisms, the influence of finite geometry on linear stability properties,[10-15] and the investigation of novel magnetic field geometries for radiation generation.[16-20] In the present analysis we make use of the quasilinear formalism developed by Dimos[1] to investigate the long-time nonlinear evolution of the free electron laser instability for a tenuous electron beam propagating in the z-direction through the helical wiggler magnetic field $\underset{\sim}{B}_0 = -\hat{B} \cos k_0 z \, \hat{\underset{\sim}{e}}_x - \hat{B} \sin k_0 z \, \hat{\underset{\sim}{e}}_y$. The theoretical model neglects longitudinal perturbations ($\delta\phi \simeq 0$) and is based on the nonlinear Vlasov-Maxwell equations for the class of beam distribution functions of the form [Eq.(2)]

$$f_b(z,\underset{\sim}{p},t) = n_0 \delta(P_x)\delta(P_y) G(z,p_z,t),$$

where $\partial/\partial x = 0 = \partial/\partial y$ is assumed, and (P_x,P_y) are the exact canonical momenta in the combined wiggler and transverse radiation fields. The analysis in Secs. 2-4 is based on the quasilinear kinetic equations derived in Ref. 1 assuming that a sufficiently broad spectrum of waves is excited.

For the special case of weak, resonant instability satisfying $|\gamma_k/\omega_k|$, $|\gamma_k/k\Delta v_z| \ll 1$, one of the principal conclusions in Ref. 1 is that the <u>fast</u> quasilinear process is plateau formation[41] with $\partial G_0/\partial p_z \to 0$ in the resonant region of velocity space where $v_z = \omega_k/k$. Here, γ_k is the growth rate, ω_k is the oscillation frequency, and

$G_0(p_z,t) = \int_{-L}^{L} (2L)^{-1} dz G(z,p_z,t)$ is the average distribution function. That analysis[1] did not address the subsequent long-time quasilinear degradation of beam energy and modification of $G_0(p_z,t)$ that occurs after plateau formation has taken place. In the present analysis, we investigate the long-time quasilinear evolution of the system in the context of a simple "water-bag" model where the distribution function $G_0(p_z,t)$ is assumed to have the rectangular form [Eq. (16) and Fig. 1]

$$G_0(p_z,t) = \begin{cases} \frac{1}{2\Delta(t)} , & |p_z - p_0(t)| \leq \Delta(t), \\ 0 , & |p_z - p_0(t)| > \Delta(t). \end{cases}$$

Here, $p_0(t)$ is the average electron momentum, and $\Delta(t)$ is the momentum spread.

Following a summary of the quasilinear formalism[1] and assumptions (Sec. 2), we derive coupled nonlinear equations (Sec. 3) which describe the self-consistent evolution of the average electron momentum $p_0(t)$ [Eq. (29)], the momentum spread $\Delta(t)$ [Eq.(25)], the amplifying wave spectrum $|\delta H_k(t)|^2$ [Eq. (14)], and the complex oscillation frequency $\omega_k(t) + i\gamma_k(t)$ [Eq. (26)]. These coupled equations are solved numerically (Sec. 4) for a wide range of system parameters, assuming that the input power spectrum $P_k(t = 0)$ [Eq. (40)] is flat and non-zero for a finite range of wavenumber k that overlaps with the region of k-space where the initial growth rate satisfies $\gamma_k(t = 0) > 0$. To summarize the qualitative features of the quasilinear evolution (Figs. 5-8), as the wave spectrum amplifies it is found that there is a concommitant

decrease in the mean electron energy $\gamma_0(t)mc^2 = [m^2c^4 + e^2\hat{B}^2/k_0^2 + p_0^2(t)c^2]^{\frac{1}{2}}$, an increase in the momentum spread $\Delta(t)$, and a downshift of the growth rate $\gamma_k(t)$ to lower k-values. After sufficient time has elapsed, the growth rate γ_k has downshifted sufficiently far in k-space that the region where $\gamma_k > 0$ no longer overlaps the region where the initial power spectrum $P_k(t=0)$ is non-zero. Therefore, the wave spectrum saturates, and $\gamma_0(t)$ and $\Delta(t)$ approach their asymptotic values.

It is found that the efficiency of energy extraction from the electron beam is enhanced by: (a) increasing the beam density $(\omega_p^2/c^2k_0^2)$, (b) increasing the wiggler field strength $(\hat{\omega}_c^2/c^2k_0^2)$, (c) decreasing the initial momentum spread $(\Delta/p_0)_{t=0}$, and (d) increasing the width of the input power spectrum $P_k(t=0)$. Here $\omega_p^2 = 4\pi n_0 e^2/\bar{\gamma}m$ is the plasma frequency-squared, $\hat{\omega}_c = e\hat{B}/\bar{\gamma}mc$ is the cyclotron frequency, and $\lambda_0 = 2\pi/k_0$ is the wiggler wavelength. For the cases studied in Sec. 4, the net efficiency of radiation generation $(\hat{\eta})$ is relatively low (several percent). Nonetheless, by appropriate choice of system parameters, the output power easily reaches the five MW/cm^2 range (Figs. 6-8), amplifying from an initial level of $P_k(t=0) = 100kW/cm^2$.

2. THEORETICAL MODEL AND ASSUMPTIONS

A. Introduction

In the present analysis, we investigate free electron laser radiation generation by a tenuous electron beam propagating in the z-direction perpendicular to a helical wiggler magnetic field

$$\underset{\sim}{B}_0 = -\hat{B}\cos k_0 z \hat{\underset{\sim}{e}}_x - \hat{B}\sin k_0 z \hat{\underset{\sim}{e}}_y \ , \tag{1}$$

where $\hat{B}$ = const. is the wiggler amplitude and $\lambda_0 = 2\pi/k_0$ is the wavelength. The quasilinear model[1] is based on the nonlinear Vlasov-Maxwell equations for the class of beam distribution functions of the form

$$f_b(z,\underset{\sim}{p},t) = n_0 \delta(P_x)\delta(P_y)G(z,p_z,t) \ . \tag{2}$$

Here, $\partial/\partial x = 0 = \partial/\partial y$ is assumed, and

$$P_x = p_x - \frac{e\hat{B}}{ck_0}\cos k_0 z - \frac{e}{c}\delta A_x(z,t) \ ,$$

$$P_y = p_y - \frac{e\hat{B}}{ck_0}\sin k_0 z - \frac{e}{c}\delta A_y(z,t) \ , \tag{3}$$

are the exact canonical momenta in the combined wiggler and transverse radiation fields. Moreover, in Eq. (2), n_0 = const. is the ambient electron density, -e is the electron charge, c is the speed of light in vacuo, $\underset{\sim}{p} = \gamma m \underset{\sim}{v}$ is the mechanical momentum, $\gamma mc^2 = (m^2c^4 + c^2\underset{\sim}{p}^2)^{1/2}$ is the energy, m is the electron rest mass, and the

perturbed electromagnetic fields are expressed in terms of $\delta\underset{\sim}{A}(\underset{\sim}{x},t) = \delta A_x(z,t)\hat{\underset{\sim}{e}}_x + \delta A_y(z,t)\hat{\underset{\sim}{e}}_y$ by $\delta\underset{\sim}{B} = [\hat{\underset{\sim}{e}}_z(\partial/\partial z)]\times\delta\underset{\sim}{A}$ and $\delta\underset{\sim}{E} = (-c^{-1}\partial/\partial t)\delta\underset{\sim}{A}$. The electron beam is assumed to be sufficiently tenuous that equilibrium self fields are negligibly small. In addition, it is assumed that the Compton-regime approximation is valid with negligibly small perturbations in the longitudinal electric field ($\delta\phi\simeq 0$).

The theoretical model used in Secs. 2-4 is based on the quasilinear kinetic equations derived in Ref. 1 assuming that a broad spectrum of waves is excited. The quasilinear kinetic equations describe the self-consistent nonlinear evolution of the system for perturbations about the (slowly varying) average distribution function

$$G_0(p_z,t) = \frac{1}{2L}\int_{-L}^{L} dz G(z,p_z,t) \ , \tag{4}$$

where 2L is the periodicity length in the z-direction. Moreover, the spatial dependence of the perturbed distribution function and electromagnetic field perturbations is Fourier decomposed according to

$$\delta\psi(z,t) = \sum_{k=-\infty}^{\infty} \delta\psi_k(t)\exp(ikz) \ , \tag{5}$$

where $k=2\pi n/L$, and n is an integer.

B. Quasilinear Dispersion Relation

In the quasilinear analysis, the time dependence of perturbed quantities is assumed to be of the form

$$\exp\{-i\int_0^t [\omega_k(t') + i\gamma_k(t')]dt'\} \ , \tag{6}$$

in circumstances where the time variation of $G_0(p_z,t)$ is sufficiently slow. In Eq. (6), the complex oscillation frequency $\omega_k(t) + i\gamma_k(t)$ satisfies the conjugate symmetries

$$\omega_{-k} = -\omega_k \ , \qquad \gamma_{-k} = \gamma_k \ , \tag{7}$$

and it is assumed that $\gamma_k > 0$, corresponding to temporal growth. For slowly varying $G_0(p_z,t)$, the complex oscillation frequency $\omega_k(t) + i\gamma_k(t)$ is determined self-consistently from the quasilinear dispersion relation[1]

$$D_{k+k_0}D_{k-k_0} = -\frac{1}{2}\frac{\hat{\omega}_c^2}{c^2k_0^2}\left(D_{k+k_0}+D_{k-k_0}\right) \times \left[\alpha_3\omega_p^2 + \bar{\gamma}mc^2\omega_p^2\gamma^{-2}\int \frac{dp_z}{\gamma^2}\,\frac{k\partial G_0/\partial p_z}{\omega_k - kv_z + i\gamma_k}\right], \tag{8}$$

where $\bar{\gamma}mc^2$ is a (yet unspecified) energy scale factor, $\omega_p = (4\pi n_0 e^2/\bar{\gamma}m)^{1/2}$ is the relativistic plasma frequency, $\hat{\omega}_c = e\hat{B}/\bar{\gamma}mc$ is the relativistic cyclotron frequency, α_3 is defined by $\alpha_3 = \bar{\gamma}^{-3}\int dp_z\gamma^{-3}G_0$, and γmc^2 is the electron energy in the equilibrium wiggler field, where γ is defined by

$$\gamma = \left(1 + \frac{p_z^2}{m^2c^2} + \frac{e^2\hat{B}^2}{m^2c^4k_0^2}\right)^{1/2} . \tag{9}$$

Moreover, the transverse dielectric functions $D_{k\pm k_0}(\omega_k+i\gamma_k)$ appearing in Eq. (8) are defined by

$$D_{k+k_0}(\omega_k+i\gamma_k) = (\omega_k+i\gamma_k)^2-c^2(k+k_0)^2-\alpha_1\omega_p^2 ,$$
$$D_{k-k_0}(\omega_k+i\gamma_k) = (\omega_k+i\gamma_k)^2-c^2(k-k_0)^2-\alpha_1\omega_p^2 , \tag{10}$$

where $\alpha_1 = \bar{\gamma}\int dp_z\gamma^{-1}G_0$. Note also that the effective susceptibility defined by

$$\chi_k(\omega_k+i\gamma_k) = \bar{\gamma}mc^2\omega_p^{2-2}\int \frac{dp_z}{\gamma^2}\frac{k\partial G_0/\partial p_z}{\omega_k-kv_z+i\gamma_k} , \tag{11}$$

occurs in the quasilinear dispersion relation (8).

The dispersion relation (8) determines the complex oscillation frequency $\omega_k(t) + i\gamma_k(t)$ adiabatically in time as $G_0(p_z,t)$ evolves in response to the amplifying field perturbations (Sec. 2.C). Keep in mind that the derivation of Eq. (8) has assumed that the electron beam is sufficiently tenuous that the Compton-regime approximation is valid ($\delta\phi \simeq 0$).

C. Quasilinear Kinetic Equations

To complete the quasilinear description, Eq. (8) is supplemented by coupled kinetic equations for the average distribution function $G_0(p_z,t)$ and the spectral energy density of the amplifying field perturbations.[1] In particular, $G_0(p_z,t)$ evolves according to[1]

$$\frac{\partial}{\partial t}G_0(p_z,t) = \frac{\partial}{\partial p_z}\left[D(p_z,t)\frac{\partial}{\partial p_z}G_0(p_z,t)\right] , \tag{12}$$

where the diffusion coefficient $D(p_z,t)$ is defined by

$$D(p_z,t) = 2\pi e^{2-2\gamma}\left(\frac{\hat{\omega}_c^2}{c^2k_0^2}\right)\sum_k \frac{i|\delta H_k|^2}{\gamma^2(\omega_k - kv_z + i\gamma_k)} \quad , \tag{13}$$

for $\gamma_k > 0$. Here, the normalized spectral energy density $|\delta H_k(t)|^2$ evolves according to the wave kinetic equation[1]

$$\frac{\partial}{\partial t}|\delta H_k|^2 = 2\gamma_k(t)|\delta H_k|^2 \quad , \tag{14}$$

and $|\delta H_k|^2$ is defined in terms of the perturbed vector potential by

$$|\delta H_k(t)|^2 = \frac{k^2}{8\pi}|\delta A_x(k+k_0,t)+i\delta A_y(k+k_0,t) + \delta A_x(k-k_0,t) - i\delta A_y(k-k_0,t)|^2 \quad . \tag{15}$$

Equations (8) and (12) - (14) constitute a closed description of the quasilinear evolution of the system including wave amplification [Eq. (14)], concommitant redistribution of particles in momentum space [Eqs. (12) and (13)], and self-consistent modification of linear growth properties [Eq. (8)]. A detailed derivation of the quasilinear model is presented in Ref. 1, together with a discussion of general properties of the kinetic equations, conservation laws, etc. In this regard, we note that the vector potential amplitudes in Eq. (15) carry the correct physical dimensions, whereas the vector potential amplitudes in Ref. 1 are defined in dimensionless form.

3. QUASILINEAR EVOLUTION OF THE FREE ELECTRON LASER INSTABILITY

For the special case of weak, resonant instability satisfying $|\gamma_k/\omega_k|$, $|\gamma_k/k\Delta v_z| << 1$, one of the principal conclusions in Ref. 1 is that the fast quasilinear process is plateau formation, with $\partial G_0/\partial p_z \to 0$ in the resonant region of velocity space where $v_z = \omega_k/k$. That analysis[1] did not address the subsequent long-time quasilinear degradation of beam energy and modification of $G_0(p_z,t)$ that occurs after plateau formation has taken place. In the present analysis, we investigate the long-time quasilinear evolution of the system in the context of a simple "water-bag" model where the distribution function $G_0(p_z,t)$ is assumed to have the rectangular form (Fig. 1)

$$G_0(p_z,t) = \begin{cases} \dfrac{1}{2\Delta(t)} , & |p_z - p_0(t)| \le \Delta(t) , \\ 0 , & |p_z - p_0(t)| > \Delta(t) . \end{cases} \tag{16}$$

Here, $p_0(t)$ is the average momentum,

$$\langle p_z \rangle = \int_{-\infty}^{\infty} dp_z p_z G_0(p_z,t) = p_0(t) , \tag{17}$$

and the half-width $\Delta(t)$ is related to the root-mean-square momentum spread by

$$\left\langle (p_z - \langle p_z \rangle)^2 \right\rangle = \int_{-\infty}^{\infty} dp_z (p_z - \langle p_z \rangle)^2 G_0(p_z,t) = \frac{1}{3}\Delta^2(t) . \tag{18}$$

Note in Eq. (16) that the normalization is $\int_{-\infty}^{\infty} dp_z G_0(p_z,t) = 1$, a property that is preserved by the diffusion equation (12). Also note from Eq. (16) and Fig. 1 that $G_0(p_z,t)$ is flat (independent of p_z) over the interval $p_0(t) - \Delta(t) \le p_z \le p_0(t) + \Delta(t)$, and equal to zero outside of this interval.

The self-consistent evolution of $p_0(t)$ and $\Delta(t)$ is determined by taking the appropriate momentum moments of the quasilinear kinetic equation (12) corresponding to Eqs. (17) and (18). For example, multiplying Eq. (12) by p_z and integrating over p_z gives

$$\frac{d}{dt} p_0(t) = - \int_{-\infty}^{\infty} dp_z \, D \frac{\partial G_0}{\partial p_z} , \tag{19}$$

where

$$\frac{\partial G_0}{\partial p_z} = \frac{1}{2\Delta(t)} \left\{ \delta\{p_z - [p_0(t)-\Delta(t)]\} - \delta\{p_z - [p_0(t)+\Delta(t)]\} \right\} \tag{20}$$

follows from Eq. (16). It is convenient to define the energy and axial velocity corresponding to $p_z = p_0(t) \pm \Delta(t)$ by

$$\gamma_{\pm}(t) = \left\{ 1 + \frac{e^2 \hat{B}^2}{m^2 c^4 k_0^2} + \frac{[p_0(t) \pm \Delta(t)]^2}{m^2 c^2} \right\}^{1/2} , \tag{21}$$

and

$$v_{\pm}(t) = \frac{p_0(t) \pm \Delta(t)}{\gamma_{\pm}(t) m} . \tag{22}$$

Then, substituting Eqs. (13) and (20) - (22) into Eq. (19), readily gives

$$\begin{aligned} \frac{d}{dt} p_0(t) = -2\pi e^2 \gamma^{-2} \left(\frac{\hat{\omega}_c}{c k_0} \right)^2 \sum_k \frac{i |\delta H_k|^2}{2\Delta(t)} \\ \times \left\{ \frac{1}{\gamma_-^2 (\omega_k - k v_- + i\gamma_k)} - \frac{1}{\gamma_+^2 (\omega_k - k v_+ + i\gamma_k)} \right\} , \end{aligned} \tag{23}$$

which describes the evolution of $p_0(t)$ in response to the amplifying field perturbations. Moreover, making use of Eqs. (12) and (18) gives for the evolution of $\Delta(t)$

$$\Delta(t)\frac{d}{dt}\Delta(t) = -3p_0(t)\frac{d}{dt}p_0(t) - 3\int_{-\infty}^{\infty} dp_z p_z D\frac{\partial G_0}{\partial p_z} . \tag{24}$$

Substituting Eqs. (13), (20), and (23) into Eq. (24), we obtain

$$\frac{d}{dt}\Delta(t) = 6\pi e^2\gamma^{-2}\left(\frac{\hat{\omega}_c}{ck_0}\right)^2\sum_k \frac{i|\delta H_k|^2}{2\Delta(t)} \times\left\{\frac{1}{\gamma_-^2(\omega_k-kv_-+i\gamma_k)}+\frac{1}{\gamma_+^2(\omega_k-kv_++i\gamma_k)}\right\} . \tag{25}$$

Equation (25) describes the quasilinear evolution of $\Delta(t)$ in response to the amplifying field perturbations. In addition to the wave kinetic equation (14) for $|\delta H_k|^2$, the remaining equation in the quasilinear description is the dispersion relation (8). Substituting Eq. (20) into Eq. (8) gives

$$D_{k+k_0}D_{k-k_0} = -\frac{1}{2}\frac{\hat{\omega}_c^2}{c^2k_0^2}\left[D_{k+k_0}+D_{k-k_0}\right] \times\left\{\alpha_3\omega_p^2 + \mp\gamma mc^2\omega_p^{2-2}\gamma\frac{k}{2\Delta}\left[\frac{1}{\gamma_-^2(\omega_k-kv_-+i\gamma_k)}-\frac{1}{\gamma_+^2(\omega_k-kv_++i\gamma_k)}\right]\right\} , \tag{26}$$

which determines the complex oscillation frequency $\omega_k(t)+i\gamma_k(t)$ in terms of $\Delta(t)$, $\gamma_\pm(t)$, $v_\pm(t)$ and other system parameters.

To summarize, for the choice of rectangular distribution function in Eq. (16) (so-called "water-bag" model), the self-consistent quasilinear evolution of the electron beam and radiation field is described by the closed system of coupled nonlinear equations:

Eq. (23) for the average momentum $p_0(t)$; Eq. (25) for the momentum spread $\Delta(t)$; Eq. (14) for the spectral energy density $|\delta H_k|^2$; and Eq. (26) for the complex oscillation frequency $\omega_k(t) + i\gamma_k(t)$. Equations (14), (23), (25) and (26), of course must be supplemented by the definitions of $\gamma_\pm(t)$ [Eq. (21)], $v_\pm(t)$ [Eq. (22)], $D_{k\pm k_0}$ [Eq. (10)], and $|\delta H_k|^2$ [Eq. (15)]. For specified initial conditions, Eqs. (14), (23), (25), and (26) can be used to calculate numerically (Sec. 4) the self-consistent evolution of $p_0(t)$, $\Delta(t)$, and the amplifying wave spectrum.

Finally, the dispersion relation (26) can be used to simplify the expression for dp_0/dt in Eq. (23). Dividing Eq. (26) by $(D_{k+k_0}+D_{k-k_0})$ and multiplying by $\sum_{k=-\infty}^{\infty} (i/k)|\delta H_k|^2 \ldots$ gives

$$\sum_k \frac{i|\delta H_k|^2}{k} \frac{D_{k+k_0} D_{k-k_0}}{(D_{k+k_0}+D_{k-k_0})}$$

$$= -\frac{1}{2}\gamma^{-3} mc^2 \omega_p^2 \left(\frac{\hat{\omega}_c}{ck_0}\right)^2 \sum_k \frac{i|\delta H_k|^2}{2\Delta} \tag{27}$$

$$\times \left\{ \frac{1}{\gamma_-^2(\omega_k - kv_- + i\gamma_k)} - \frac{1}{\gamma_+^2(\omega_k - kv_+ + i\gamma_k)} \right\}.$$

Combining Eqs. (27) and (23) readily gives

$$n_0 \frac{d}{dt} p_0(t) = \sum_k \frac{i|\delta H_k|^2}{kc^2} \frac{D_{k+k_0} D_{k-k_0}}{(D_{k+k_0}+D_{k-k_0})}, \tag{28}$$

for dp_0/dt. Making use of the conjugate symmetries $D_{k+k_0}(\omega_{-k}+i\gamma_{-k}) = D^*_{k-k_0}(\omega_k+i\gamma_k)$, $D_{k-k_0}(\omega_{-k}+i\gamma_{-k}) = D^*_{k+k_0}(\omega_k+i\gamma_k)$, $\omega_{-k}=-\omega_{-k}$ and $\gamma_{-k} = \gamma_k$, the k-summation in Eq. (28) can be further simplified to give

$$n_0 \frac{d}{dt} \bar{p}_0(t) = -2 \sum_k |\delta H_k|^2 \frac{\omega_k \gamma_k}{kc^2} \tag{29}$$

$$\times \frac{\{|D_{k+k_0}|^2 + |D_{k-k_0}|^2\}}{|D_{k+k_0} + D_{k-k_0}|^2} ,$$

which is exactly equivalent to Eqs. (23) and (28). Replacing Eq. (23) by Eq. (29), the numerical analysis in Sec. 4 is based on the coupled quasilinear equations (14), (25), (26), and (29).

4. NUMERICAL RESULTS

A. Introduction and Definitions

The coupled system of nonlinear equations (14), (25), (26), and (29) have been solved numerically for a broad range of system parameters. In this section, we summarize typical numerical results for both moderately high-energy and low-energy electron beams. In this regard, it is convenient to introduce the notation

$$\gamma_0(t) \equiv \left[1 + \frac{e^2\hat{B}^2}{m^2c^4k_0^2} + \frac{p_0^2(t)}{m^2c^2}\right]^{1/2} . \tag{30}$$

From Eqs. (9), (17), and (30), it is evident that $\gamma_0(t)mc^2$ corresponds to the energy of an electron moving with the average axial momentum $p_0(t)$ of the electron beam. In addition, we take the (heretofore unspecified) energy scale factor $\bar{\gamma}mc^2$ that occurs in the quasilinear equations and related definitions to be equal to the initial value of γ_0, i.e.,

$$\bar{\gamma} \equiv \gamma_0(t=0) . \tag{31}$$

The corresponding average axial velocity V_b of a beam electron at t=0 is given by

$$V_b \equiv \frac{p_0(t=0)}{\bar{\gamma}m} . \tag{32}$$

For future reference, as a useful estimate of where the free electron laser radiation spectrum is excited, we consider the dispersion relation (26) at t=0 in the limiting case of a "cold" electron beam with $\Delta \to 0$. For right-circularly polarized electromagnetic waves with

$D_{k-k_0} \simeq 0$, strong interaction between the beam electrons and the radiation field occurs in Eq. (26) for frequency and wavenumber (ω_s, k_s) satisfying the simultaneous resonance conditions

$$\omega_s^2 - c^2(k_s-k_0)^2 - \alpha_1\omega_p^2 = 0 \ ,$$
$$\omega_s - k_s V_b = 0 \ . \tag{33}$$

For a tenuous electron beam with $\alpha_1\omega_p^2 << c^2k_s^2$, the upshifted (high-frequency) branch in Eq. (33) satisfies $\omega_s = c(k_s-k_0)$ and $\omega_s = k_s V_b$. Solving for k_s then gives $k_s = k_0/(1-V_b/c)$, or equivalently,

$$k_s = \frac{\bar{\gamma}^{-2}(1+\beta_b)}{1+\bar{\gamma}^{-2}\hat{\omega}_c^2/c^2k_0^2}\, k_0 \ , \tag{34}$$

where $\beta_b = V_b/c$, $\hat{\omega}_c = e\hat{B}/\bar{\gamma}mc$, and use has been made of $1-V_b^2/c^2 = \bar{\gamma}^{-2} + \hat{\omega}_c^2/c^2k_0^2$. For sufficiently small wiggler amplitude that $\bar{\gamma}^{-2}\hat{\omega}_c^2/c^2k_0^2 << 1$, Eq. (34) gives the familiar result $k_s \simeq \bar{\gamma}^{-2}(1+\beta_b)k_0$. For example, for $\bar{\gamma}=10$, $\beta_b \simeq 1$ and $\bar{\gamma}^{-2}\hat{\omega}_c^2/c^2k_0^2 << 1$, Eq. (34) gives $k_s \simeq 200\ k_0$. On the other hand, for $\bar{\gamma}=10$, $\beta_b \simeq 1$ and $\bar{\gamma}^{-2}\hat{\omega}_c^2/c^2k_0^2 = 0.773$ (the parameters chosen in Fig. 2), Eq. (34) gives $k_s \simeq 113\ k_0$.

A further important definition relates to the total electromagnetic field energy density

$$\mathcal{E}_F(t) = \sum_k \mathcal{E}_k(t) = \sum_k \frac{|\delta E_{\underset{\sim}{k}}|^2 + |\delta B_{\underset{\sim}{k}}|^2}{8\pi} \ . \tag{35}$$

Defining

$$\delta A_k^{\pm} = \delta A_x(k,t) \pm i\delta A_y(k,t) \ , \tag{36}$$

some straightforward algebra shows that $\mathcal{E}_k(t)$ can be expressed as[1]

$$\mathcal{E}_k(t) = \frac{1}{16\pi c^2}\left\{|\delta A^+_{k+k_0}|^2[|\omega_k+i\gamma_k|^2 + c^2(k+k_0)^2] + |\delta A^-_{k-k_0}|^2[|\omega_k+i\gamma_k|^2 + c^2(k-k_0)^2]\right\} . \tag{37}$$

Moreover, the vector potential amplitudes occurring in Eqs. (15) and (36) are related by[1]

$$\frac{\delta A^+_{k+k_0}}{\delta A^-_{k-k_0}} = \frac{D_{k-k_0}}{D_{k+k_0}} \ , \tag{38}$$

where $D_{k\pm k_0}$ is defined in Eq. (10).

Also of interest is the average $\delta\underset{\sim}{E}\times\delta\underset{\sim}{B}$ power flow in the z-direction defined by

$$P(t) = \frac{c}{4\pi}\int_{-L}^{L}\frac{dz}{2L}\,(\delta\underset{\sim}{E}\times\delta\underset{\sim}{B})_z = \sum_k P_k(t) \ . \tag{39}$$

Here, $P_k(t)$ can be expressed as[1]

$$P_k(t) = \frac{1}{8\pi}\left\{(k+k_0)\omega_k|\delta A^+_{k+k_0}|^2 + (k-k_0)\omega_k|\delta A^-_{k-k_0}|^2\right\} . \tag{40}$$

In the numerical analysis in Sec. 4.c, we specify the input spectrum $P_k(t=0)$, and make use of Eqs. (14), (25), (26), and (29) to follow the nonlinear evolution of the system.

Finally, for small initial momentum spread with $\Delta(0) << p_0(0)$, the initial beam kinetic energy density is approximately $(\bar{\gamma}-1)n_0mc^2$. We therefore define the dynamic (time-dependent) efficiency of radiation generation $\eta(t)$ by

$$\eta(t) = \frac{\mathcal{E}_F(t) - \mathcal{E}_F(0)}{n_0(\bar{\gamma}-1)mc^2} , \tag{41}$$

where $\mathcal{E}_F(t)$ is defined in Eq. (35). Assuming that the field energy density saturates at some level $\mathcal{E}_F(\infty)$ as $t\to\infty$, the net efficiency of radiation generation (denote by $\hat{\eta}$) is given by

$$\hat{\eta} = \eta(\infty) . \tag{42}$$

Finally, we remind the reader that the vector potential amplitudes occuring in Eqs. (36) - (40) have the correct physical dimensions, whereas the vector potential amplitudes in Ref. 1 are defined in dimensionless form.

B. Linear Growth Properties

Before analyzing the quasilinear development of the system predicted by the coupled nonlinear equations (14), (25), (26) and (29), it is useful to make use of the dispersion relation (26) to investigate (parametrically) the linear stability properties for the choice of rectangular distribution function in Eq. (16). Typical numerical results are illustrated in Figs. 2 - 4. In Figs. 2 and 3, the system parameters are chosen to be $\bar{\gamma} = 10$, $\omega_p^2/c^2k_0^2 = 1.6 \times 10^{-3}$ and $\hat{\omega}_c^2/c^2k_0^2 = 7.73 \times 10^{-3}$, corresponding to a tenuous electron beam with moderate energy. Figure 2 shows plots of the normalized growth rate γ_k/k_0c versus k/k_0 obtained from Eq. (26) for a wide range of normalized momentum spread Δ/p_0. Evidently, for very narrow momentum spread ($\Delta/p_0 = 3 \times 10^{-4}$, say), the instability growth rate is broadband with maximum growth rate centered near $k_s/k_0 \simeq 113$, as estimated from Eq. (34). On the other hand, as Δ/p_0 is increased, we note from Fig. 2 that there is a downshift in wavenumber corresponding to maximum growth. Moreover, the maximum growth rate and the instability bandwidth decrease substantially as Δ/p_0 is increased to the several percent range. This is further illustrated in Fig. 3, where Eq. (26) has been used to obtain plots of $(\gamma_k/k_0c)_{MAX}$ (normalized maximum growth rate), $(k/k_0)_{MAX}$ (normalized wavenumber at maximum growth), and $(\Delta k/k_0)$ (normalized width of γ_k at half maximum) versus Δ/p_0, for Δ/p_0 ranging from 10^{-4} to 0.3.

Figures 2 and 3 already give some indication of the qualitative features of the quasilinear evolution of the system that we can expect from a detailed analysis of the nonlinear coupled equations (14), (25), (26) and (29). For example, as the wave spectrum amplifies

[Eq.(14)], there will be a concommitant increase in $\Delta(t)/p_0(t)$ [Eqs. (25) and (29)]. Dynamically, this will result in a downshift in the growth rate curve $\gamma_k(t)$ to lower k-values, narrower bandwidth, and smaller growth rates.

Finally, in Fig. 4, we make use of the dispersion relation (26) to calculate linear stability properties for the choice of parameters $\bar{\gamma} = 1.3$, $\omega_p^2/c^2k_0^2 = 5.99 \times 10^{-3}$ and $\hat{\omega}_c^2/c^2k_0^2 = 2.25 \times 10^{-3}$, and Δ/p_0 ranging from $\Delta/p_0 = 0.2 \times 10^{-2}$ to 10^{-2}. Here, the beam energy is relatively low in comparison with Figs. 2 and 3. As expected from Eq. (34) the maximum growth rate occurs for $k_s/k_0 \simeq 2.9$. As in Figs. 2 and 3, the instability bandwidth $\Delta k/k_0$ decreases as Δ/p_0 is increased. However, for the choice of parameters in Fig. 4, Δ/p_0 has not been increased to large enough values to show a noticeable downshift in the k-value for maximum growth rate.

C. Quasilinear Evolution

The coupled nonlinear equations (14), (25), (26) and (29) have been solved numerically to determine the self-consistent quasilinear evolution of the wave spectrum $|\delta H_k(t)|^2$ [Eq. (14)], the momentum spread $\Delta(t)$ [Eq. (25)], the mean momentum $p_0(t)$ [Eq. (29)], and the complex oscillation frequency $\omega_k + i\gamma_k$ [Eq. (26)] for a wide range of system parameters. Typical numerical results are illustrated in Figs. 5-8 both for moderate beam energy ($\bar{\gamma} = 10$ in Figs. 5-7) and for low beam energy ($\bar{\gamma} = 1.3$ in Fig. 8). In Figs. 5-8, the time t is measured in units of

$$T_0 = \frac{\lambda_0}{c} = \frac{2\pi}{k_0 c}, \tag{42}$$

which is the time required for a light pulse to transverse one wiggler wavelength $\lambda_0 = 2\pi/k_0$. In addition to specifying values for $\omega_p^2/c^2k_0^2$, $\bar{\gamma} = \gamma_0(t = 0)$, $p_0(t = 0)$ and $\Delta(t = 0)$, we specify the initial power spectrum

$$P_k(t = 0)$$

as input data to the coupled nonlinear equations (14), (25), (26) and (29). In all cases (Figs. 5-8), the initial power spectrum $P_k(t =0)$ is assumed to be flat and non-zero over a finite bandwidth of wavenumber k, and equal to zero outside of this range. In particular, in Figs. 5, 6 and 8, the initial power spectrum $P_k(t =0)$ is taken to be non-zero for the range of wavenumber k exactly overlapping with the region where the <u>initial</u> growth rate satisfies $\gamma_k(0) > 0$ [compare Figs. 5(e), 6(e) and 8(e) with Figs. 5(a), 6(a) and 8(a)]. On the other hand, in Fig. 7, the bandwidth of the initial power spectrum $P_k(t = 0)$ is taken to be twice the width of the region where $\gamma_k(0) > 0$ [compare Fig. 7(e) and Fig 7(a)]. In all cases (Figs. 5-8), the value of $P_k(t = 0)$ is equal to $100 kW/cm^2$ in the region of k-space where the initial power spectrum is non-zero. Moreover, in the numerical analysis, the amplifying spectrum is divided into fifteen discrete k-values in Figs. 5, 6 and 8, and into thirty discrete k-values in Fig. 7.

We now describe the quasilinear evolution of the system, beginning with Fig. 5 where $\bar{\gamma} = 10$, $\omega_p^2/c^2k_0^2 = 1.6 \times 1.0^{-3}$, $\hat{\omega}_c^2/c^2k_0^2 = 7.73 \times 10^{-3}$ and $(\Delta/p_0)_{t=0} = 10^{-2}$. The initial power spectrum $P_k(t = 0)$ is non-zero over the interval $107.75 < k/k_0 < 113.25$ [Fig. 5(e)] where the initial growth rate satisfies $\gamma_k(t = 0) > 0$ [Fig. 5(a)]. Solving the coupled nonlinear equations (14), (25), (26) and (29), it is found that the field energy $\mathcal{E}_F(t)$ amplifies [Fig. 5(d) and Eq. (14)], which leads to a decrease in the mean electron energy $\gamma_0(t)mc^2$ [Fig. 5(b) and Eq. (29)], an

increase in the momentum spread $\Delta(t)$ [Fig. 5(c) and Eq. (25)], and a concommitant shift in the unstable region of k-space where $\gamma_k > 0$ to lower values of wavenumber [Fig. 5(a) and Eq. (26)]. Indeed, by $t/T_0 = 25$ in Fig. 5(a), the growth rate has decreased considerably and γ_k has downshifted sufficiently far in k-space that the region where $\gamma_k(t = 25T_0) > 0$ no longer overlaps the region where the initial power spectrum $P_k(t = 0)$ is non-zero [Fig. 5(e)]. Consequently, the wave spectrum saturates by $t/T_0 = 25$ [Fig 5(e)], and γ_0, Δ and $\mathcal{E}_F$ approach their asymptotic values [Figs. 5(b)-5(d)]. Moreover, the dynamic efficiency $\eta(t)$, which is defined in Eq. (41) and plotted versus t/T_0 in Fig. 5(f), approaches the value $\hat{\eta} = 1.1\%$. For the parameters chosen in Fig. 5, we note that the free electron laser instability is relatively weak, as manifest by low growth rate [Fig. 5(a)], the small amplification of the wave spectrum [Fig. 5(e)], and the low efficiency $\hat{\eta}$ [Fig. 5(f)]. Moreover, during the stabilization process, $\gamma_0(t)mc^2$ decreases by about 0.5% [Fig.5(b)], and $\Delta(t)/p_0$ increases from 1% at $t = 0$ to 2.5% at $t = 25T_0$ [Fig. 5(c)].

As an example corresponding to stronger instability, still with $\bar{\gamma} = 10$ and $(\Delta/p_0)_{t=0} = 10^{-2}$, in Fig. 6 the normalized beam density and wiggler strength are increased to $\omega_p^2/c^2k_0^2 = 8 \times 10^{-3}$ and $\hat{\omega}_c^2/c^2k_0^2 = 38.6 \times 10^{-3}$. Comparing Fig. 6 with Fig. 5, it is evident that the instability growth rate is considerably larger [Fig. 6(a)] and the wave spectrum amplifies to a much higher level [Figs. 6(d) and 6(e)]. Correspondingly, there is a larger decrease in $\gamma_0(t)mc^2$ [Fig. 6(b)] and a larger increase in $\Delta(t)/p_0$ [Fig. 6(c)], with the efficiency approaching $\hat{\eta} = 3.3\%$ in Fig. 6(f). With the larger initial growth rate in Fig. 6(a), the stabilization process in Fig. 6 occurs on a faster time scale than in Fig. 5. Indeed, by $t/T_0 = 16.5$ in Fig. 6(a), the growth rate γ_k has downshifted sufficiently far in k-space that the region where

$\gamma_k(t = 16.5T_0) > 0$ no longer overlaps the region where the initial power spectrum $P_k(t = 0)$ is non-zero [Fig. 6(e)]. Therefore, by $t/T_0 = 16.5$, the wave spectrum saturates [Fig. 6(e)], and γ_0, Δ and $\mathcal{E}_F$ approach their asymptotic values [Figs. 6(b)-6(d)]. For the parameters in Fig. 6, we note from Fig. 6(c) that the normalized momentum spread $\Delta(t)/p_0$ increases from 1% at $t = 0$ to 6.5% at $t = 16.5T_0$.

Another way to augment the energy extracted from the electron beam is to increase the width of the input power spectrum $P_k(t = 0)$. This is illustrated in Fig. 7 for the choice of system parameters $\bar{\gamma} = 10$, $\omega_p^2/c^2k_0^2 = 8 \times 10^{-3}$, $\hat{\omega}_c^2/c^2k_0^2 = 7.73 \times 10^{-3}$ and $(\Delta/p_0)_{t=0} = 10^{-2}$. Note from Fig. 7(a) that the initial growth rate satisfies $\gamma_k(t=0) > 0$ for k-values in the range $105 < k/k_0 < 120$, whereas the initial power spectrum $P_k(t = 0)$ in Fig. 7(e) is assumed to be non-zero over the wider interval $91 < k/k_0 < 120$. Therefore, the interaction time of the electron beam with the amplifying wave spectrum is prolonged because the waves continue to grow beyond the time when γ_k ceases to overlap with the region where $\gamma_k(t = 0) > 0$. Indeed, from Figs. 7(a)-7(f), the system continues to evolve dynamically until $t/T_0 = 107$, when the growth rate γ_k ceases to overlap with the region of k-space where the input power spectrum $P_k(t = 0)$ is non-zero [Figs. 7(a) and 7(e)]. During this process, the beam energy $\gamma_0(t)mc^2$ decreases [Fig. 7(b)], the momentum spread $\Delta(t)$ increases [Fig. 7(c)], the field energy and wave spectrum amplify and saturate [Figs. 7(d) and 7(e)], and the efficiency approaches $\hat{\eta} = 5.6\%$.

As a final numerical example, in Fig. 8 we consider a low-energy electron beam with $\bar{\gamma} = 1.3$, $\omega_p^2/c^2k_0^2 = 5.99 \times 10^{-3}$, $\hat{\omega}_c^2/c^2k_0^2 = 2.25 \times 10^{-3}$, and $(\Delta/p_0)_{t=0} = 5 \times 10^{-3}$. In this case, the upshifted wavenumber is

relatively small with maximum initial growth rate occurring for $k_s/k_0 \simeq 2.75$. From Figs. 8(a)-8(f), the general features of the evolution of $\gamma_0(t)$, $\Delta(t)$, $\hat{\mathcal{E}}_F(t)$, $P_k(t)$ and $\eta(t)$ are qualitatively similar to Figs. 5 and 6. For the parameters chosen in Fig. 8, the stabilization process is completed by $t/T_0 = 31.5$, when the growth rate γ_k [Fig. 8(a)] ceases to overlap with the region in k-space where the initial power spectrum $P_k(t=0)$ is non-zero [Fig. 8(e)]. From Fig. 8(f), we find that the efficiency approaches $\hat{\eta} = 5.3\%$ for the choice of system parameters in Fig. 8.

Finally, we remind the reader that parameters such as $\omega_p^2/c^2k_0^2$, $\hat{\omega}_c^2/c^2k_0^2$, etc., in the analysis in Sec. 4, are dimensionless. To provide a quantitative estimate of beam density, wiggler strength, etc., we choose (as an example) a wiggler wavelength $\lambda_0 = 6.28$ cm corresponding to $k_0 = 1\ \text{cm}^{-1}$. Then, for example, the system parameters for Fig. 5 correspond to

$$\overline{\gamma} = 10;\ \lambda_0 = 6.28\ \text{cm};\ \lambda_s = 315\ \text{microns};$$

$$\hat{B} = 1.5\ \text{kG};\ n_0 = 4.5 \times 10^9 \text{cm}^{-3};\ J_b = |n_0 e V_b| = 21.6\ \text{A/cm}^2,$$

where $\lambda_s = (1 - V_b/c)\lambda_0$ [Eq. (34)]. On the other hand, for Fig. 8, the system parameters are

$$\overline{\gamma} = 1.3;\ \lambda_0 = 6.28\ \text{cm};\ \lambda_s = 2.3\ \text{cm};$$

$$\hat{B} = 105\ \text{G};\ n_0 = 2.2 \times 10^9 \text{cm}^{-3};\ J_b = 6.7\ \text{A/cm}^2,$$

which still corresponds to a relatively tenuous beam.

5. CONCLUSIONS

In the present analysis, we have investigated the long-time quasilinear evolution of the free electron laser instability for a tenuous relativistic electron beam propagating perpendicular to a helical wiggler magnetic field. Following a summary of the quasilinear model[1] and assumptions (Sec. 2), we specialized to the case where the average distribution function $G_0(p_z,t)$ is assumed to have a rectangular form in momentum space [Eq. (16) and Fig.1]. Coupled nonlinear equations are derived (Sec. 3) which describe the self-consistent evolution of the mean electron momentum $p_0(t)$ [Eq. (29)], the momentum spread $\Delta(t)$ [Eq. (25)], the amplifying spectrum $|\delta H_k(t)|^2$ [Eq. (14)], and the complex oscillation frequency $\omega_k(t)+i\gamma_k(t)$ [Eq. (26)]. These coupled equations are solved numerically (Sec. 4) for a wide range of system parameters, assuming that the input power spectrum $P_k(t = 0)$ is flat and non-zero for a finite range of wavenumber k that overlaps with the region of k-space where the initial growth rate satisfies $\gamma_k(t = 0) > 0$. To summarize the qualitative features of the quasilinear evolution (Figs. 5-8), as the wave spectrum amplifies it is found that there is a concommitant decrease in the mean electron energy $\gamma_0(t)mc^2$, an increase in the momentum spread $\Delta(t)$, and a downshift of the growth rate $\gamma_k(t)$ to lower k-values. After sufficient time has elapsed, the growth rate γ_k has downshifted sufficiently far in k-space that the region where $\gamma_k(t) > 0$ no longer overlaps the region where the initial power spectrum $P_k(t = 0)$ is non-zero. Therefore, the wave spectrum saturates, and $\gamma_0(t)$ and $\Delta(t)$ approach their asymptotic values. It is found that the efficiency of energy extraction from the electron beam is enhanced by: (a) increasing the beam density $(\omega_p^2/c^2k_0^2)$, (b) increasing the wiggler field strength $(\hat{\omega}_c^2/c^2k_0^2)$, (c) decreasing

the initial momentum spread $(\Delta/p_0)_{t=0}$, and (d) increasing the width of the input power spectrum $P_k(t = 0)$. For the cases studied in Sec. 4, the net efficiency of radiation generation ($\hat{\eta}$) was relatively low (several percer Nonetheless, by appropriate choice of system parameters, the output power easily reaches the five MW/cm^2 range (Figs. 6-8), amplifying from an initial level of $P_k(t = 0) = 100\ kW/cm^2$.

Finally, for the quasilinear model to be valid, it is necessary that the amplifying wave spectrum be sufficiently broad in k-space that the autocorrelation time for the waves (τ_{ac}) be short in comparison with the characteristic time scale for quasilinear relaxation (τ_{rel}).[1] We estimate $\tau_{ac} \sim |\Delta(\omega_k - kv_z)|^{-1} \sim |(c - V_b)\Delta k|^{-1}$, where $V_b = p_0(t=0)/\bar{\gamma}m$ is the average beam velocity, and Δk is the characteristic width of the amplifying k-spectrum. We also estimate τ_{rel} by $\tau_{rel} \sim 2(\gamma_k)^{-1}_{MAX}$, corresponding to a few maximum growth times. Then, the inequality $\tau_{ac} << \tau_{rel}$ can be expressed as

$$\left(\frac{\gamma_k}{ck_0}\right)_{MAX} << 2\left(\frac{\Delta k}{k_s}\right), \tag{43}$$

where $k_s \simeq k_0/(1-V_b/c)$ is the characteristic wavenumber at maximum growth. That is, the wave spectrum must be sufficiently broad and the growth rate sufficiently weak in order for the quasilinear model in Secs. 2 - 4 to be valid, and for coherence effects (such as particle trapping in the ponder-motive potential) to be unimportant in the nonlinear evolution of the system. Inspection of the numerical results in Figs. 5 - 8 readily shows that the inequality in Eq. (43) is satisfied (to within a factor of ten or more) for the range of system parameters investigated in Sec. 4.

In conclusion, it has been noted that the efficiency of radiation generation is typically in the several percent range, at least within the present quasilinear model which assumes an oscillator configuration (temporal growth) with constant wiggler amplitude $\hat{B}$ = const. One way to increase the efficiency is to "time-taper" the magnetic wiggler amplitude $\hat{B}$ in such a way that the region of instability ($\gamma_k > 0$) continues to overlap with the region where the input power spectrum $P_k(t=0)$ is non-zero. To illustrate with a simple model, consider the case where the momentum spread Δ is sufficiently small that $k_s \simeq k_0(1-V_z/c)^{-1}$ is a good estimate of the wavenumber at maximum growth. Here $V_z(t) = p_0(t)/\gamma_0(t)m$ is the axial beam velocity. Evidently, a decrease in beam velocity ΔV_z causes a downshift in k_s by an amount $\Delta k_s = (1 - V_z/c)^{-2}\Delta V_z$. Moreover, the velocity change ΔV_z is related to the momentum change Δp_0 and energy change $\Delta\gamma_0$ by $\Delta V_z = (\gamma_0 mc)^{-1}[\Delta p_0 - p_0\Delta\gamma_0/\gamma_0]$. Therefore, making use of $\gamma_0^2 = 1 + e^2\hat{B}^2/m^2c^4k_0^2 + p_0^2/m^2c^2$, where $\hat{B}(t)$ is allowed to vary, we obtain $\gamma_0\Delta\gamma_0 = e^2\hat{B}\Delta\hat{B}/m^2c^4k_0^2 + p_0\Delta p_0/m^2c^2$, and find that ΔV_z can be expressed as

$$\Delta V_z = \frac{mc}{p_0}\left(1 - \frac{p_0^2}{\gamma_0^2 m^2 c^2}\right)\Delta\gamma_0 - \frac{mc}{p_0}\,\frac{e^2\hat{B}}{\gamma_0 m^2 c^4 k_0^2}\,\Delta\hat{B}. \tag{44}$$

Because $\Delta k_s = (1 - V_z/c)^{-2}\Delta V_z$, in order to prevent a downshift in k_s (i.e., maintain $\Delta k_s \simeq 0$), we allow $\hat{B}$ to vary in such a manner that $\Delta V_z = 0$ in Eq. (44). Defining $a_w = e\hat{B}/mc^2k_0$, and making use of the definition of γ_0, the condition $\Delta V_z = 0$ can be expressed as $a_w^2\hat{B}^{-1}\Delta\hat{B} = (1 + a_w^2)\,\gamma_0^{-1}\Delta\gamma$, or in terms of the time derivatives of $\hat{B}$ and γ_0,

$$\frac{1}{\hat{B}}\frac{d}{dt}\hat{B} = \left(\frac{1 + a_w^2}{a_w^2}\right)\frac{1}{\gamma_0}\frac{d\gamma_0}{dt}. \tag{45}$$

Equation (45) can be interpreted as follows. As the wave spectrum amplifies there is a corresonding (quasilinear) decrease in $\gamma_0(t)$. If, in addition, the temporal evolution of the wiggler amplitude B is taylored in such a way that Eq. (45) is satisfied, then the beam velocity V_z remains unchanged ($\Delta V_z = 0$), and there is no downshift in k_s ($\Delta k_s = 0$). The sustained overlap of $\gamma_k(t)$ with the input power spectrum will then lead to higher efficiencies. Equation (45) is the temporal analogue of spatial-tapering of the magnetic wiggler for the case of an amplifier (spatial growth).

ACKNOWLEDGMENTS

It is a pleasure to acknowledge the benefit of useful discussions with Jonathan Wurtele. This research was supported by the Office of Naval Research and in part by the National Science Foundation.

REFERENCES

1. A.M. Dimos and R.C. Davidson, "Quasilinear Stabilization of the Free Electron Laser Instability for a Relativistic Electron Beam Propagating through a Transverse Helical Wiggler Magnetic Field," submitted for publication (1984).
2. B. Lane and R.C. Davidson, Phys. Rev. A27, 2008 (1983).
3. R.C. Davidson and W.A. McMullin, Phys. Rev. A26, 410 (1982).
4. N.S. Ginzburg and M.A. Shapiro, Opt. Comm. 40, 215 (1982).
5. T. Taguchi, K. Mima, and T. Mochizuki, Phys. Rev. Lett. 46, 824 (1981).
6. N.M. Kroll, P.L. Morton, and M.N. Rosenbluth, IEEE J. Quantum Electron. QE-17, 1436 (1981).
7. P. Sprangle, C.M. Tang, and W.M. Manheimer, Phys. Rev. A21, 302 (1980).
8. W.H. Louisell, J.F. Lam, D.A. Copeland, and W.B. Colson, Phys. Rev. A19, 288 (1979).
9. F.A. Hopf, P. Meystre, M.O. Scully, and W.H. Louisell, Phys. Rev. Lett. 37, 1342 (1976).
10. H.P. Freund and A.K. Ganguly, Phys. Rev. A28, 3438 (1983).
11. R.C. Davidson and Y.Z. Yin, Phys. Rev. A30, in press (1984).
12. G.L. Johnston and R.C. Davidson, J. Appl. Phys. 55,]285 (1984).
13. H.S. Uhm and R.C. Davidson, Phys. Fluids 26, 288 (1983).
14. R.C. Davidson and H.S. Uhm, J. Appl. Phys. 53, 2910 (1982).
15. H.S. Uhm and R.C. Davidson, Phys. Fluids 24, 2348 (1981).
16. R.C. Davidson, W.A. McMullin and K. Tsang, Phys. Fluids 27, 233 (1983).
17. R.C. Davidson and W.A. McMullin, Phys. Fluids 26, 840 (1983).
18. R.C. Davidson and W.A. McMullin, Phys. Rev. A26, 1997 (1982).
19. W.A. McMullin and G. Bekefi, Phys. Rev. A25, 1826 (1982).
20. W.A. McMullin and G. Bekefi, Appl. Phys. Lett. 39, 845 (1981).
21. W.B. Colson, IEEE J. Quant. Electron. QE17, 1417 (1981).

22. R.C. Davidson and H.S. Uhm, Phys. Fluids 23, 2076 (1980).

23. P. Sprangle and R.A. Smith, Phys. Rev. A21, 293 (1980).

24. I.B. Bernstein and J.L. Hirshfield, Physica (Utrecht) 20A, 1661 (1979).

25. T. Kwan and J.M. Dawson, Phys. Fluids 22, 1089 (1979).

26. N.M. Kroll and W.A. McMullin, Phys. Rev. A17, 300 (1978).

27. T. Kwan, J.M. Dawson, and A.T. Lin, Phys. Fluids 20, 581 (1977).

28. A. Haseqawa, Bell Syst. Tech. J. 57, 3069 (1978).

29. W.B. Colson, Phys. Lett. 59A, 187 (1976).

30. J. Fajans, G. Bekefi, Y.Z. Yin and B. Lax, Phys. Rev. Lett. 53, 246 (1984).

31. G. Bekefi, R.E. Shefer and W.W. Destler, Appl. Phys. Lett. 44, 280 (1983).

32. C.W. Roberson, J.A. Pasour, F. Mako, R.F. Lucey Jr., and P. Sprangle, Infrared and Millimeter Waves 10, 361 (1983), and references therein.

33. A. Grossman, T.C. Marshall and S.P. Schlesinger, Phys. Fluids 26, 337 (1983).

34. D. Prosnitz and A.M. Sessler, in Physics of Quantum Electronics (Addison-Wesley, Reading, Mass.) 9, 651 (1982).

35. R.K. Parker, R.H. Jackson, S.H. Gold, H.P. Freund, V.L. Grnatstein, P.C. Efthimion, M. Herndon, and A.K. Kinkead, Phys. Rev. Lett. 48. 238 (1982).

36. S. Benson, D.A.G. Deacon, J.N. Eckstein, J.M.J. Madey, K. Robinson, T.I. Smith, and R. TAber, Phys. Rev. Lett. 48, 235 (1982).

37. A.N. Didenko, A.R. Borisov, G.R. Fomenko, A.V. Kosevnikov, G.V. Melnikov, Yu G. Stein, and A.G. Zerlitsin, IEEE Trans. Nucl. Sci. 28, 3169 (1981).

38. D.B. McDermott, T.C. Marshall, S.P. Schlesinger, R.K. Parker, and V.L. Granatstein, Phys. Rev. Lett. 41, 1368 (1978).

39. D.A.G. Deacon, L.R. Elias, J.M.J. Madey, G.J. Ramian, H.A. Schwettman, and T.I. Smith, Phys. Rev. Lett. 38, 892 (1977).

40. L.R. Elias, W.M. Fairbank, J.M.J. Madey, H.A. Schwettman, and T.I. Smith, Phys. Rev. Lett. 36, 717 (1976).

41. R.C. Davidson, Methods in Nonlinear Plasma Theory (Academic Press, New York, 1972).

FIGURE CAPTIONS

Fig. 1 Plot of $G_0(p_z,t)$ versus p_z for the choice of rectangular distribution function in Eq. (16) .

Fig. 2 Plot of normalized growth rate γ_k/k_0c versus k/k_0 obtained from Eq. (26) for $\bar{\gamma} = 10$, $\omega_p^2/c^2k_0^2 = 1.6\times10^{-3}$, $\hat{\omega}_p^2/c^2k_0^2 = 7.73 \times 10^{-3}$, and several values of Δ/p_0.

Fig. 3 Plots of normalized maximum growth rate, $(\gamma_k/k_0c)_{MAX}$, normalized wavenumber at maxiumum growth, $(k/k_0)_{MAX}$, and normalized width of γ_k at half maxiumum, $\Delta k/k_0$, versus Δ/p_0 obtained from Eq. (26) for $\bar{\gamma} = 10$, $\omega_p^2/c^2k_0^2 = 1.6 \times 10^{-3}$ and $\hat{\omega}_c^2/c^2k_0^2 = 7.73 \times 10^{-3}$.

Fig. 4 Plot of normalized growth rate γ_k/k_0c versus k/k_0 obtained from Eq. (26) for $\bar{\gamma} = 1.3$, $\omega_p^2/c^2k_0^2 = 5.99 \times 10^{-3}$, $\hat{\omega}_c^2/c^2k_0^2 = 2.25 \times 10^{-3}$ and several values of Δ/p_0.

Fig. 5 Quasilinear time development determined from Eqs. (14). (25), (26) and (29) for $\bar{\gamma} = 10$, $\omega_p^2/c^2k_0^2 = 1.6 \times 10^{-3}$, $\hat{\omega}_c^2/c^2k_0^2 = 7.73\times10^{-3}$ and $(\Delta/p_0)_{t=0} = 10^{-2}$. Shown are plots of (a) normalized growth rate $\gamma_k(t)/k_0c$ versus k/k_0, (b) mean electron energy $\gamma_0(t)$ versus t/T_0, (c) normalized momentum spread $\Delta(t)/p_0$ versus t/T_0, (d) normalized field energy $\mathcal{E}_F(t)/\mathcal{E}_F(0)$ versus t/T_0, (e) power spectrum $P_k(t)$ versus k/k_0, and (f) dynamic efficiency $\eta(t)$ versus t/T_0. The input power is $P_k(t = 0) = 100kW/cm^2$ over the interval $107.75 < k/k_0 < 113.25$ [Fig. 5(e)].

Fig. 6 Quasilinear time development determined from Eqs. (14), (25), (26) and (29) for $\bar{\gamma} = 10$, $\omega_p^2/c^2k_0^2 = 8 \times 10^{-3}$, $\hat{\omega}_c^2/c^2k_0^2 = 38.6 \times 10^{-3}$ and $(\Delta/p_0)_{t=0} = 10^{-2}$. Shown are plots of (a) normalized growth rate $\gamma_k(t)/k_0c$ versus k/k_0, (b) mean electron energy $\gamma_0(t)$ versus t/T_0, (c) normalized momentum spread $\Delta(t)/p_0$ versus t/T_0, (d) normalized field energy $\mathcal{E}_F(t)/\mathcal{E}_F(0)$ versus t/T_0, (e) power spectrum $P_k(t)$ versus k/k_0, and (f) dynamic efficiency $\eta(t)$ versus t/T_0. The input power is $P_k(t=0) = 100\text{kW/cm}^2$ over the interval $36.75 < k/k_0 < 53.25$ [Fig. 6(e)].

Fig. 7 Quasilinear time development determined from Eqs. (14), (25), (26) and (29) for $\bar{\gamma} = 10$, $\omega_p^2/c^2k_0^2 = 8 \times 10^{-3}$, $\hat{\omega}_c^2/c^2k_0^2 = 7.73 \times 10^{-3}$ and $(\Delta/p_0)_{t=0} = 10^{-2}$. Shown are plots of (a) normalized growth rate $\gamma_k(t)/k_0c$ versus k/k_0, (b) mean electron energy $\gamma_0(t)$ versus t/T_0, (c) normalized momentum spread $\Delta(t)/p_0$ versus t/T_0, (d) normalized field energy $\mathcal{E}_F(t)/\mathcal{E}_F(0)$ versus t/T_0, (e) power spectrum $P_k(t)$ versus k/k_0, and (f) dynamic efficiency $\eta(t)$ versus t/T_0. The input power is $P_k(t = 0) = 100\,\text{kW/cm}^2$ over the interval $91 < k/k_0 < 120$ [Fig. 7(e)].

Fig. 8 Quasilinear time development determined from Eqs. (14). (25), (26) and (29) for $\bar{\gamma} = 1.3$, $\omega_p^2/c^2k_0^2 = 5.99 \times 10^{-3}$, $\hat{\omega}_c^2/c^2k_0^2 = 2.25 \times 10^{-3}$ and $(\Delta p_0)_{t=0} = 5 \times 10^{-3}$. Shown are plots of (a) normalized growth rate $\gamma_k(t)/k_0c$ versus k/k_0, (b) mean electron energy $\gamma_0(t)$ versus t/T_0, (c) normalized momentum spread $\Delta(t)/p_0$ versus t/T_0, (d) normalized field energy $\mathcal{E}_F(t)/\mathcal{E}_F(0)$ versus t/T_0, (e) power spectrum $P_k(t)$ versus k/k_0, and (f) dynamic efficiency $\eta(t)$ versus t/T_0. The input power is $P_k(t) = 100\,\mathrm{kW/cm^2}$ over the interval $2.68 < k/k_0 < 3.45$ [Fig. 8(e)].

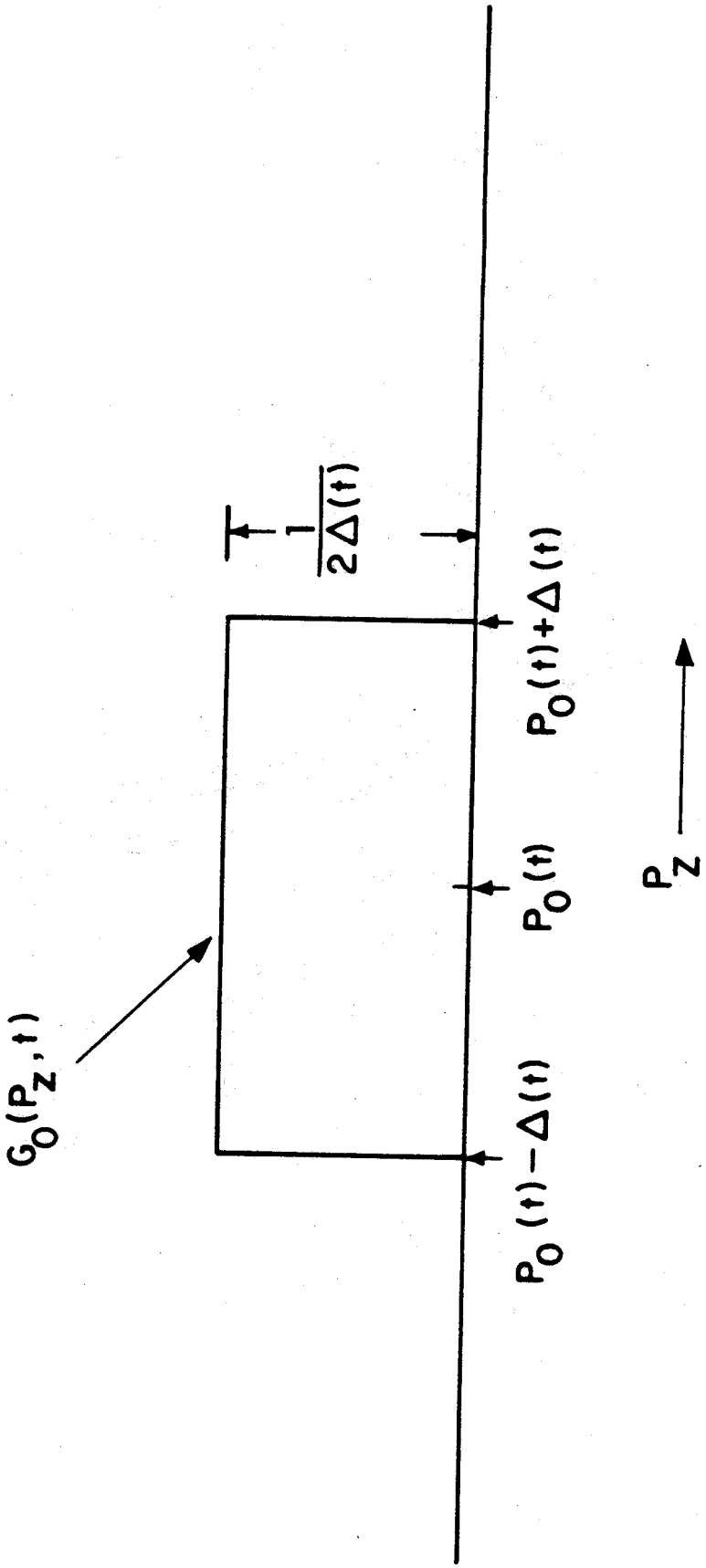

Fig. 1

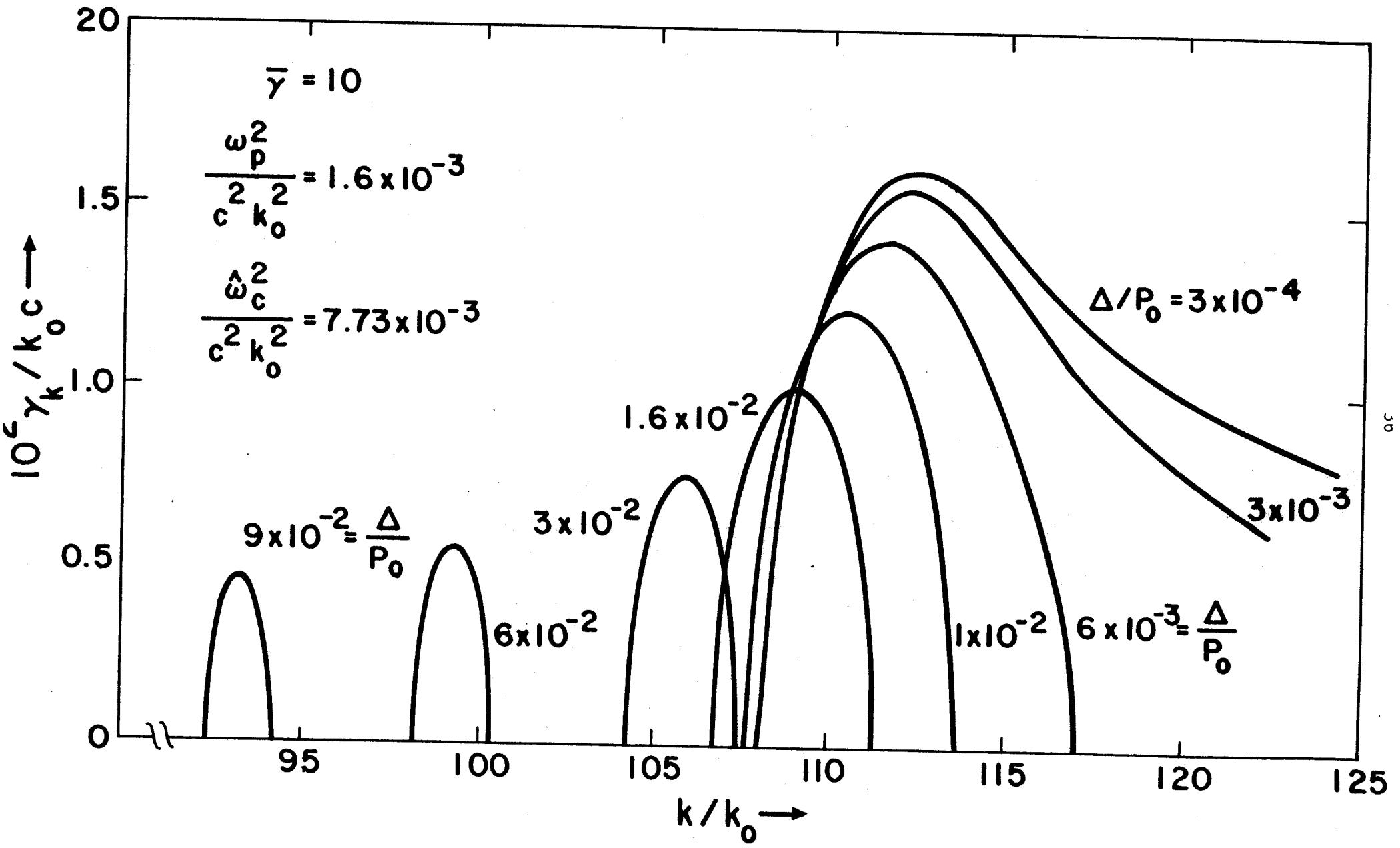
20
1.5
1.0
0.5
0
$\bar{\gamma} = 10$
$\frac{\omega_p^2}{c^2 k_0^2} = 1.6 \times 10^{-3}$
$\frac{\hat{\omega}_c^2}{c^2 k_0^2} = 7.73 \times 10^{-3}$
$10^2 \gamma_k / k_0 c \longrightarrow$
$\Delta/P_0 = 3 \times 10^{-4}$
3×10^{-3}
1.6×10^{-2}
3×10^{-2}
$9 \times 10^{-2} = \frac{\Delta}{P_0}$
6×10^{-2}
1×10^{-2}
$6 \times 10^{-3} = \frac{\Delta}{P_0}$
95
100
105
110
115
120
125
$k/k_0 \longrightarrow$

Fig. 2

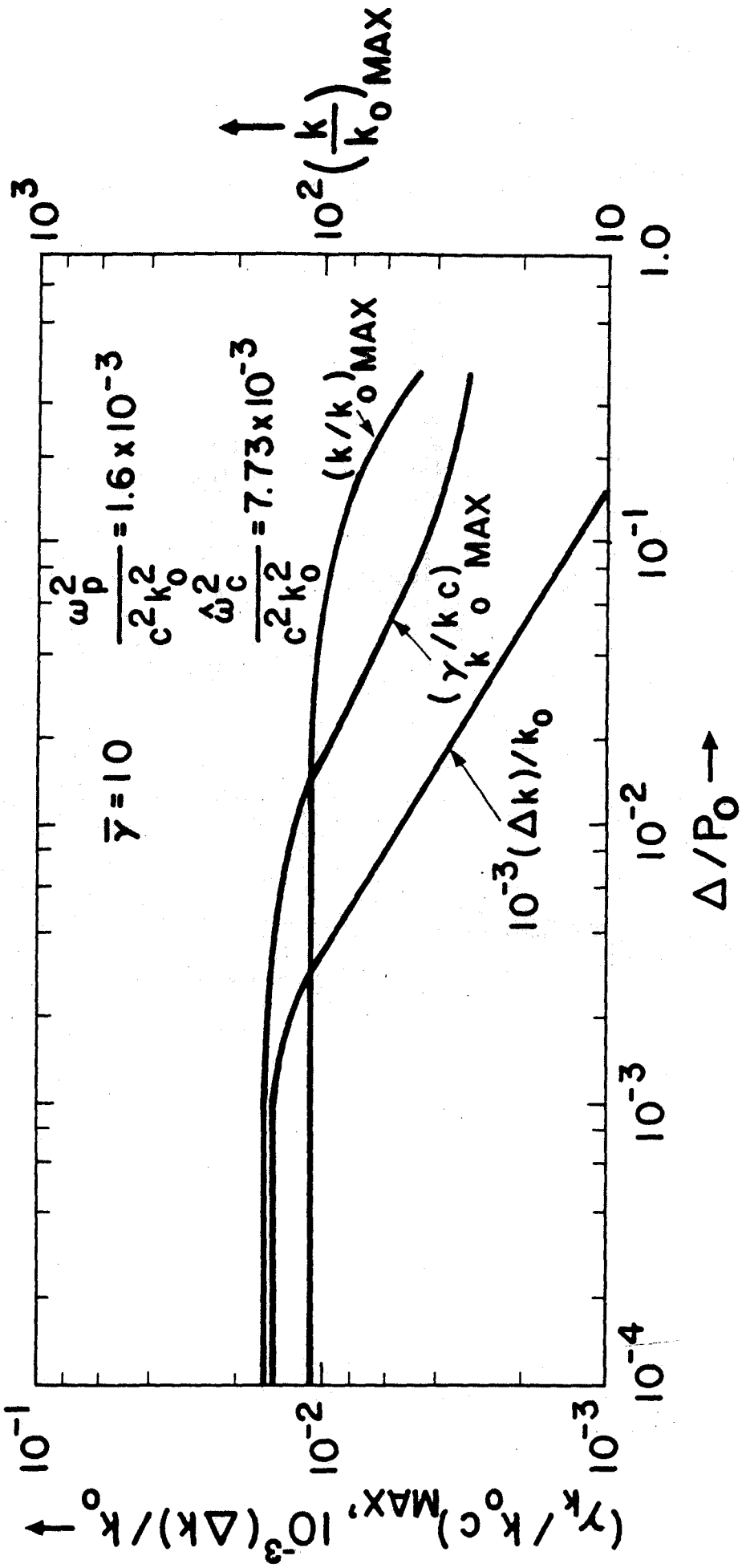
10^3
$10^2\left(\frac{k}{k_o}\right)_{MAX}$
10
1.0
$\frac{\omega_p^2}{c^2k_o^2} = 1.6\times10^{-3}$
$\frac{\hat{\omega}_c^2}{c^2k_o^2} = 7.73\times10^{-3}$
$(k/k_o)_{MAX}$
$\bar{\gamma} = 10$
$(\gamma_k/k_o c)_{MAX}$
$10^{-3}(\Delta k)/k_o$
10^{-1}
10^{-2}
10^{-3}
10^{-4}
$\Delta/P_o \rightarrow$
$(\gamma_k/k_o c)_{MAX}, 10^{-3}(\Delta k)/k_o \rightarrow$

Fig. 3

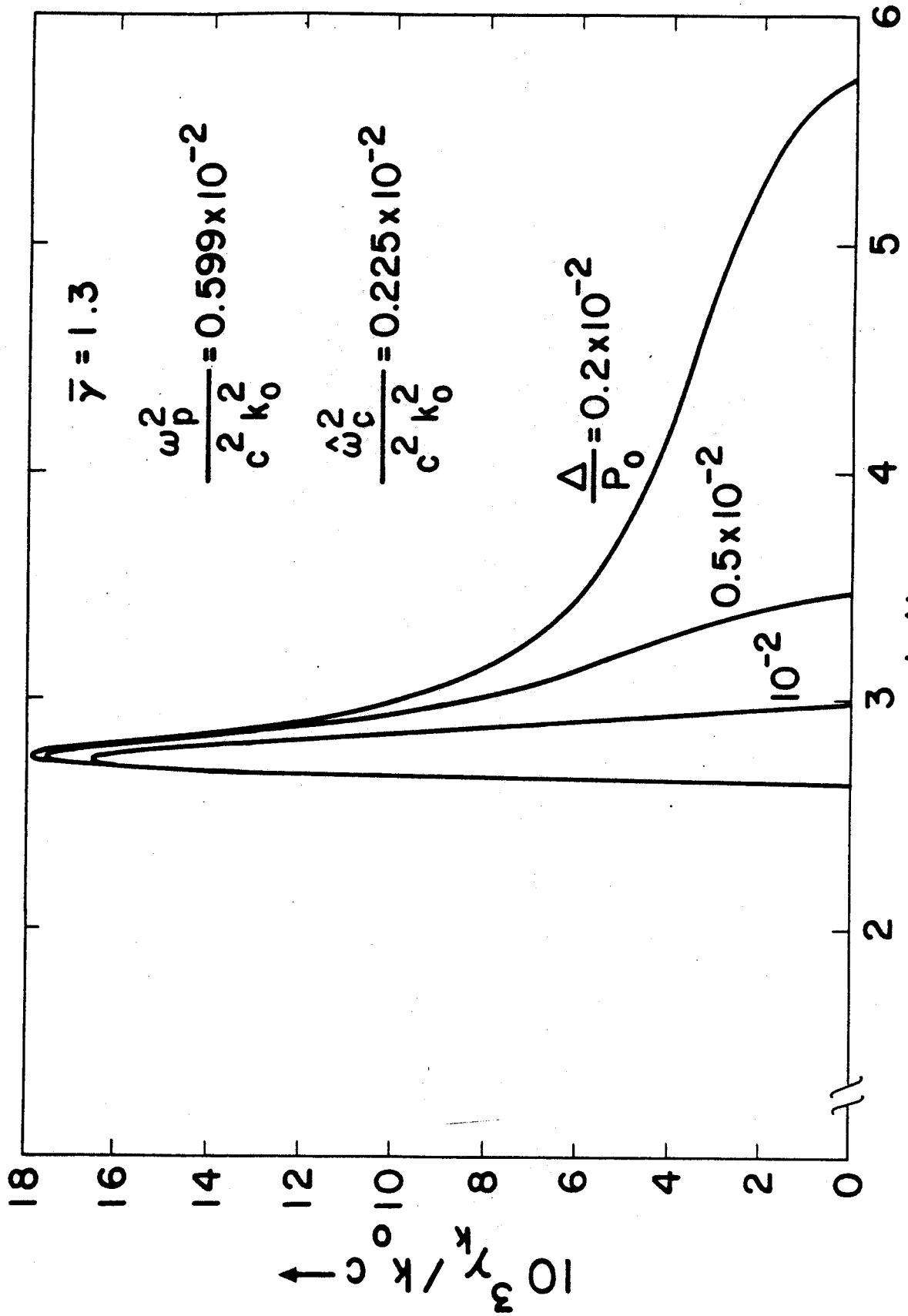
$\bar{\gamma} = 1.3$
$\frac{\omega_p^2}{c^2 k_o^2} = 0.599 \times 10^{-2}$
$\frac{\hat{\omega}_c^2}{c^2 k_o^2} = 0.225 \times 10^{-2}$
$\frac{\Delta}{P_o} = 0.2 \times 10^{-2}$
0.5×10^{-2}
10^{-2}
$10^3 \gamma_k / k_o c \longrightarrow$
$k / k_o \longrightarrow$
0
2
4
6
8
10
12
14
16
18
2
3
4
5
6

Fig. 4

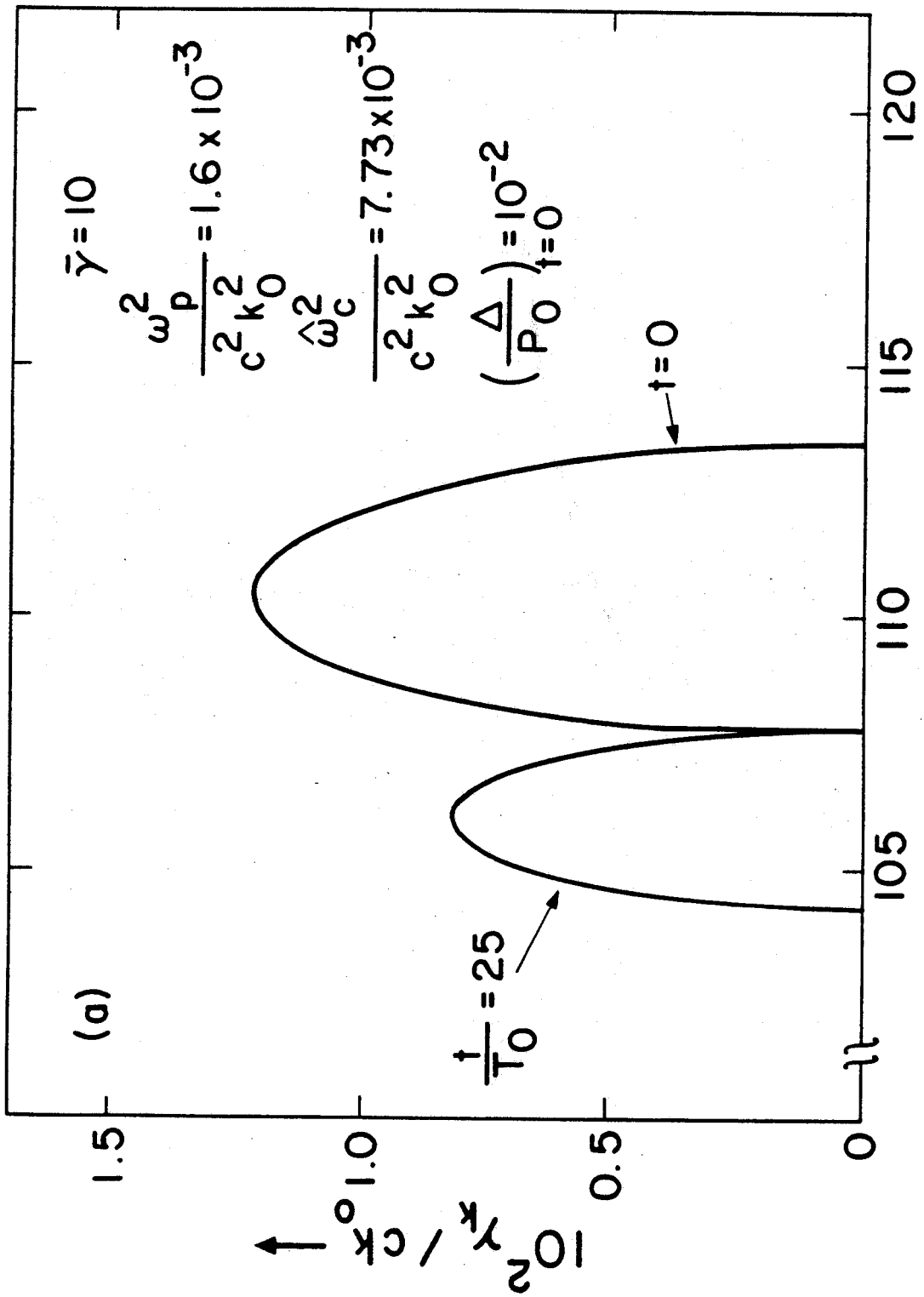
(a)
$\bar{\gamma}=10$
$\frac{\omega_p^2}{c^2k_0^2}=1.6\times10^{-3}$
$\frac{\hat{\omega}_c^2}{c^2k_0^2}=7.73\times10^{-3}$
$\left(\frac{\Delta}{P_0}\right)_{t=0}=10^{-2}$
$\frac{t}{T_0}=25$
t=0
$10^2\gamma_k/ck_0$
k/k_0
0
0.5
1.0
1.5
105
110
115
120

Fig. 5(a)

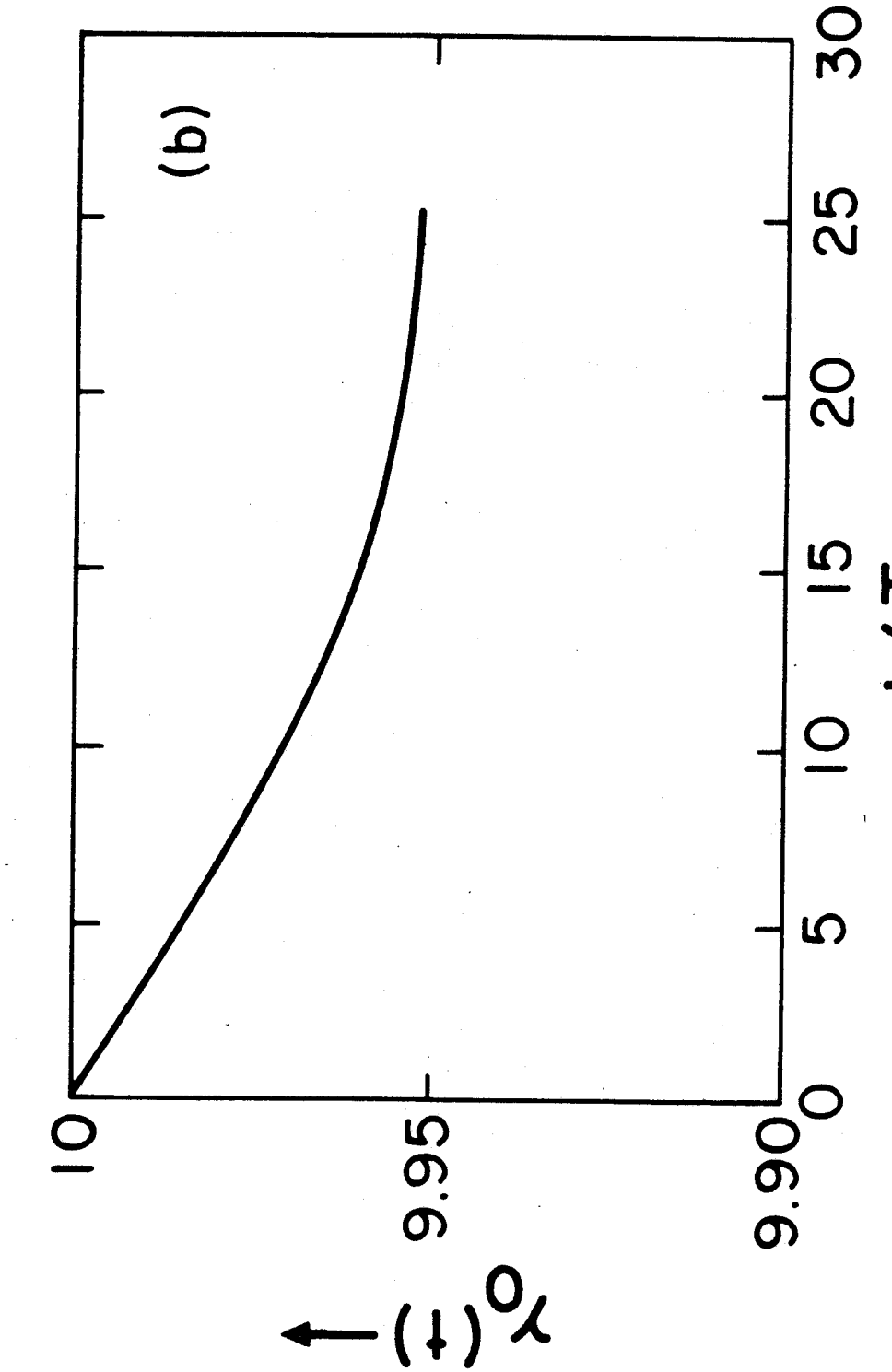

Fig. 5(b)

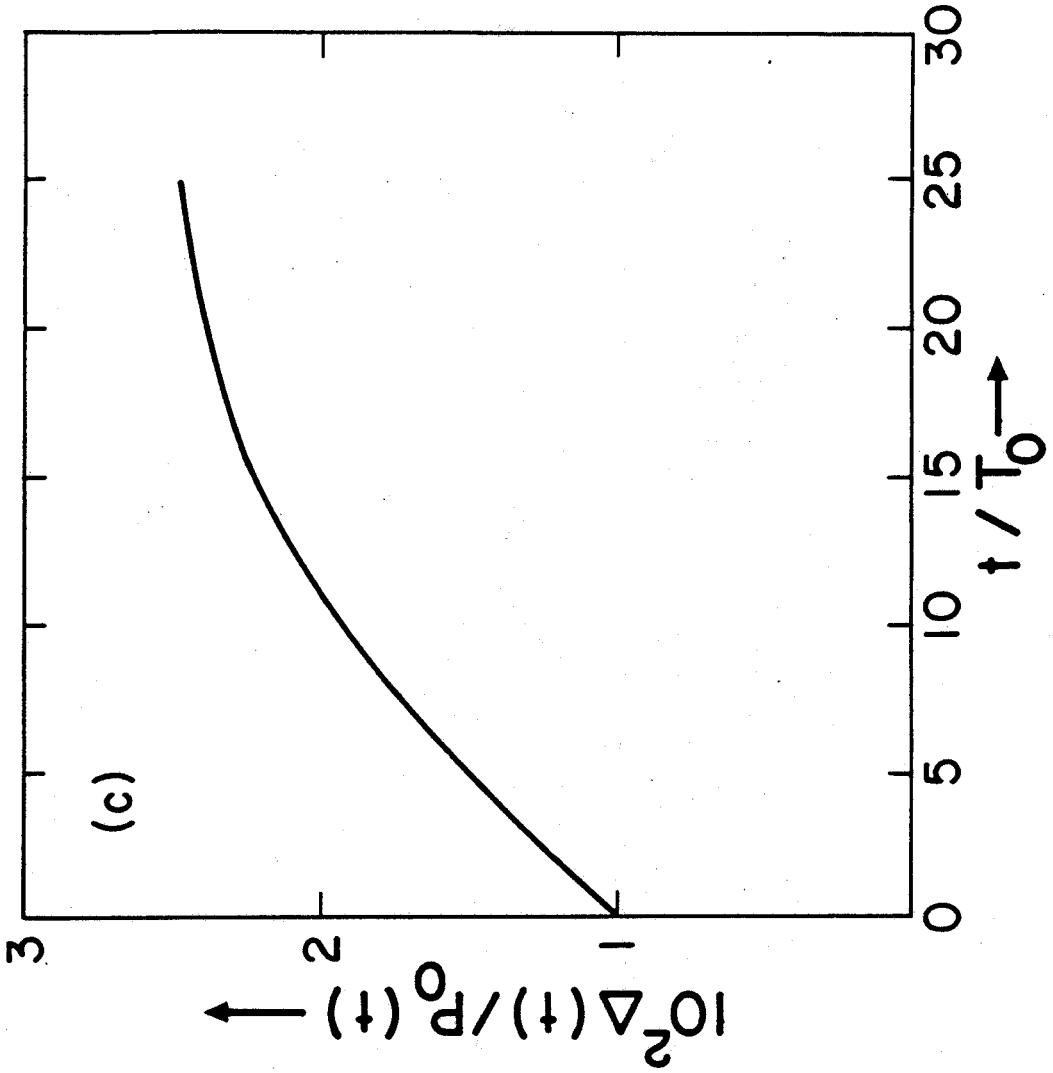

Fig. 5(c)

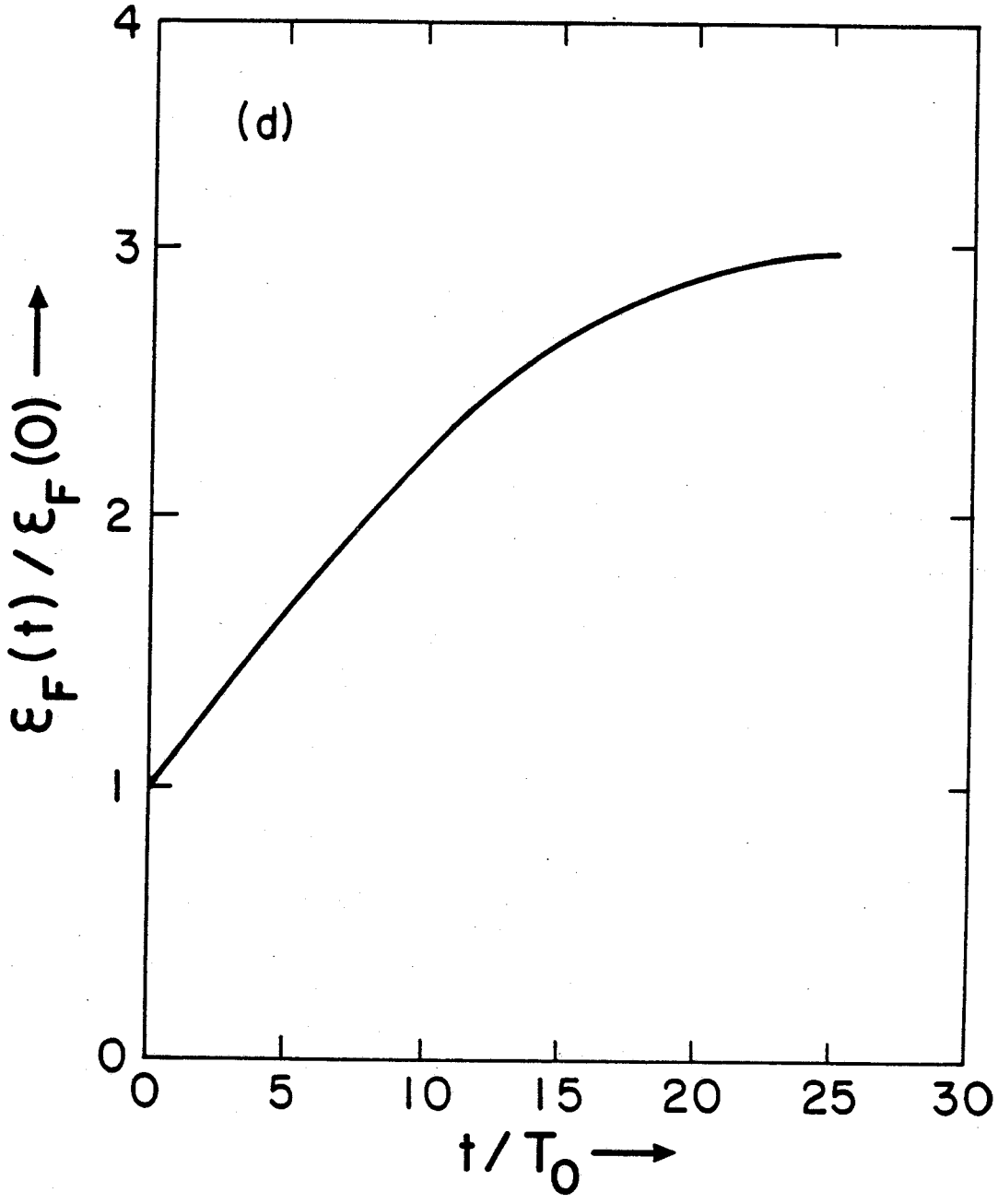

Fig. 5(d)

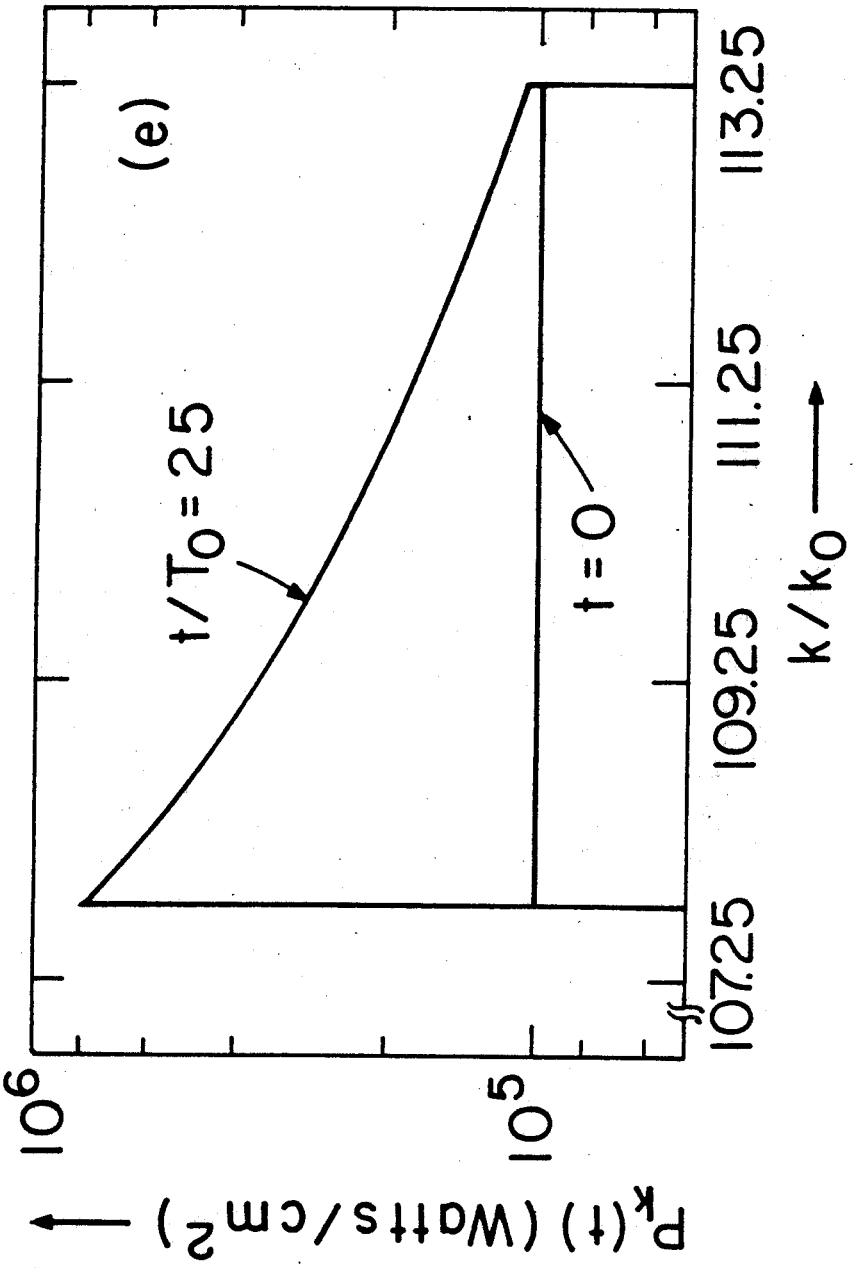

Fig. 5(e)

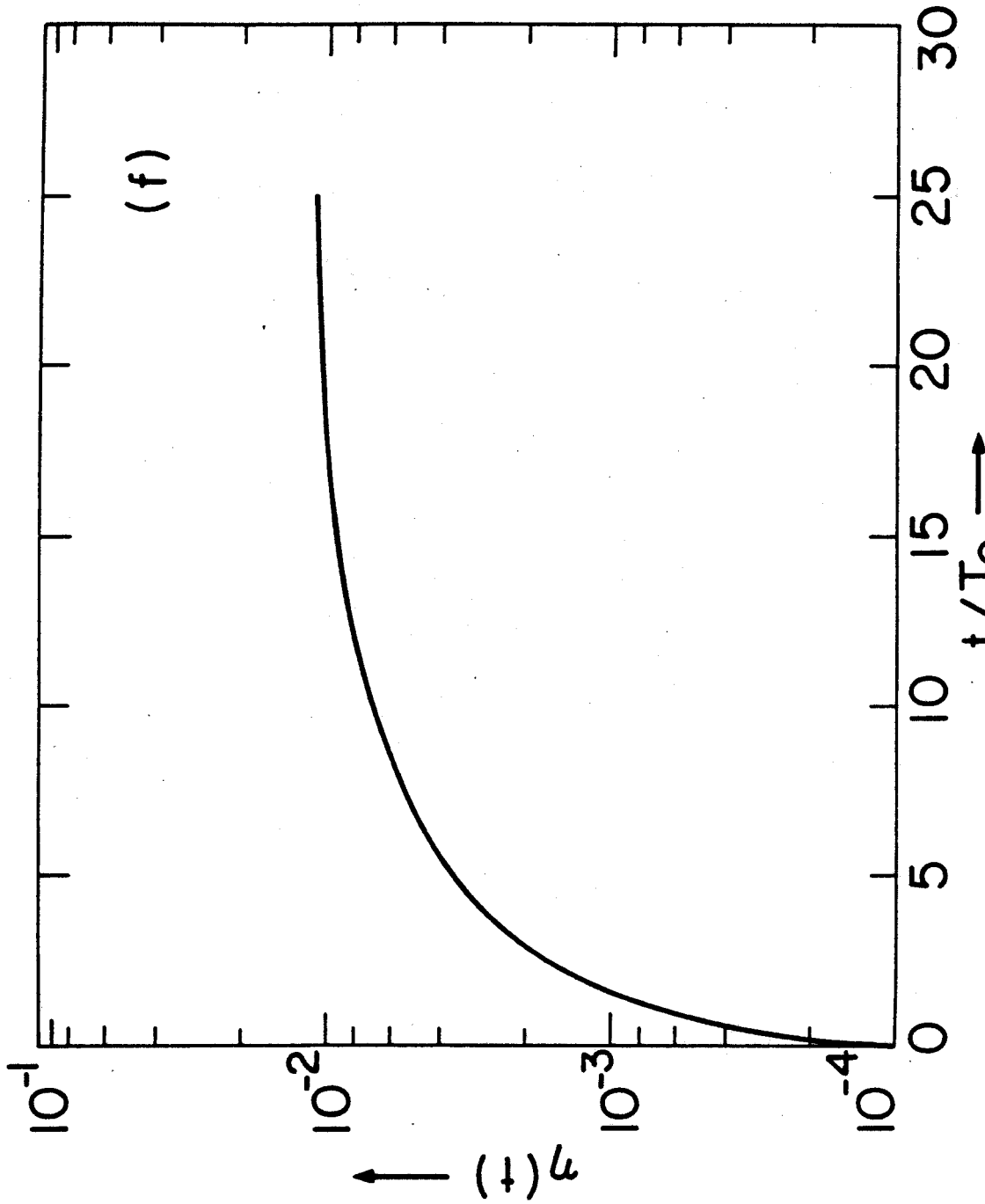

Fig. 5(f)

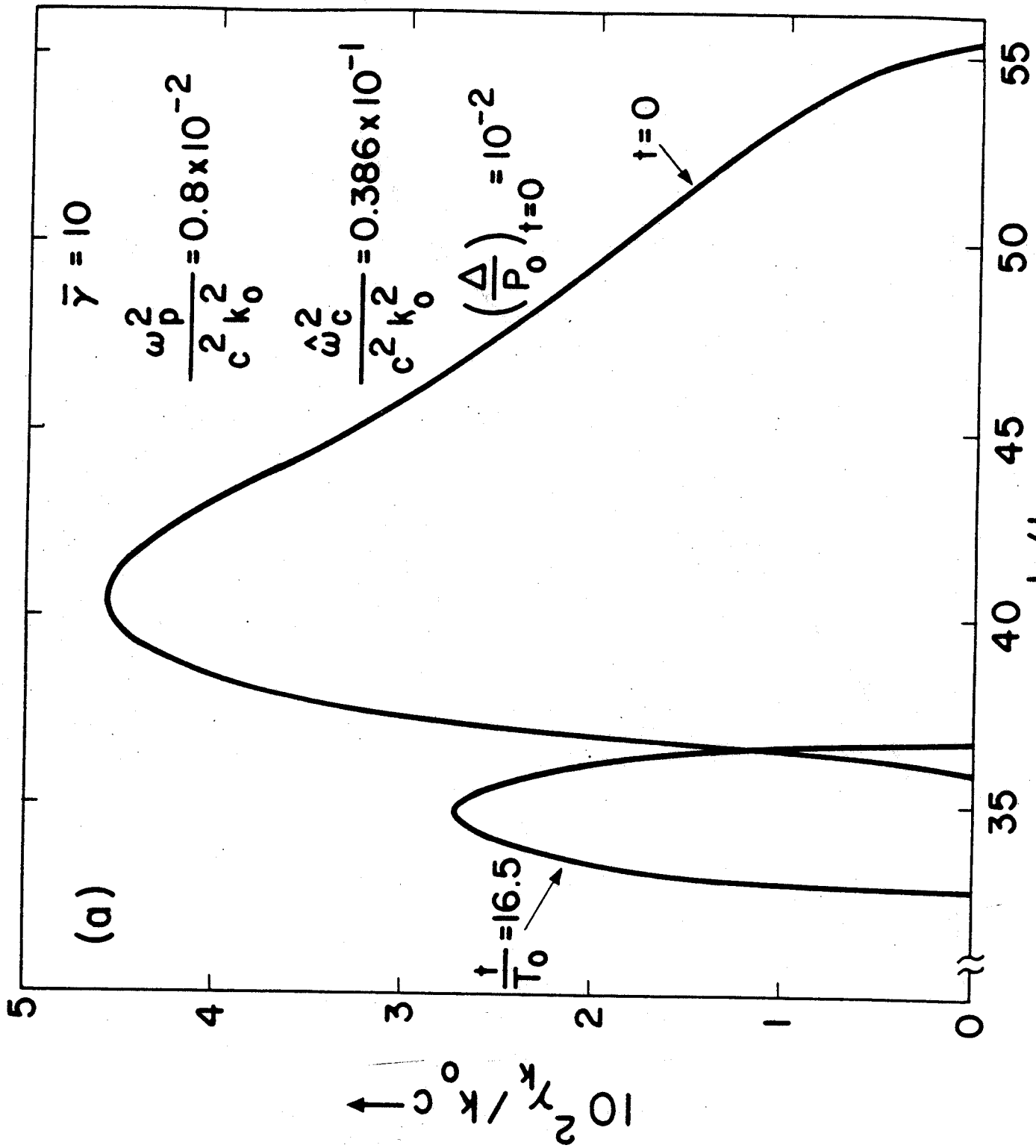
$10^2 \gamma_k / k_o c$
k / k_o
$\bar{\gamma} = 10$
$\frac{\omega_p^2}{c^2 k_o^2} = 0.8 \times 10^{-2}$
$\frac{\hat{\omega}_c^2}{c^2 k_o^2} = 0.386 \times 10^{-1}$
$\left(\frac{\Delta}{P_o}\right)_{t=0} = 10^{-2}$
t=0
$\frac{t}{T_o} = 16.5$
(a)

Fig. 6(a)

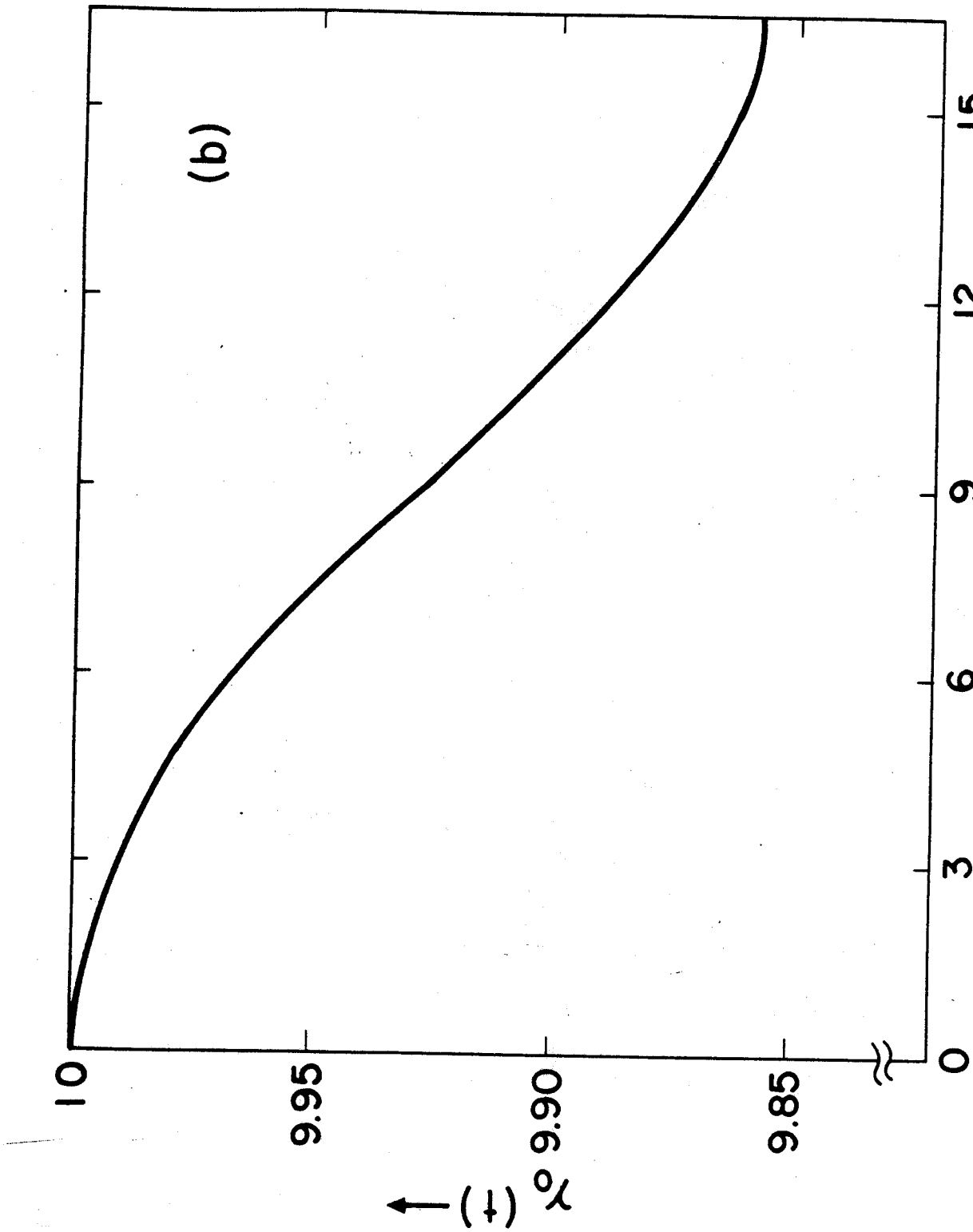

Fig. 6(b)

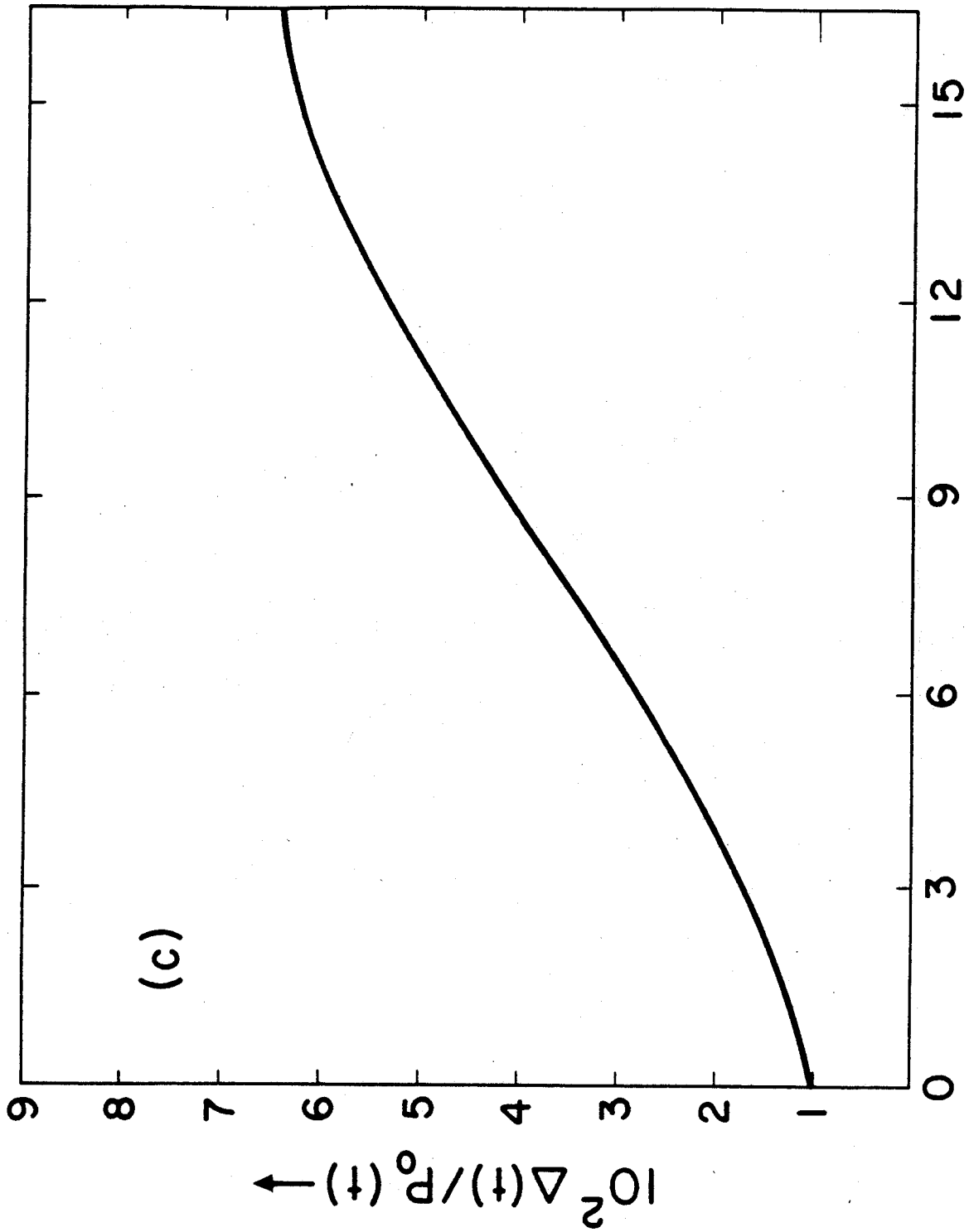
(c)
$10^2 \Delta(t)/P_o(t) \longrightarrow$
$t/T_o \longrightarrow$
0
3
6
9
12
15
1
2
3
4
5
6
7
8
9

Fig. 6(c)

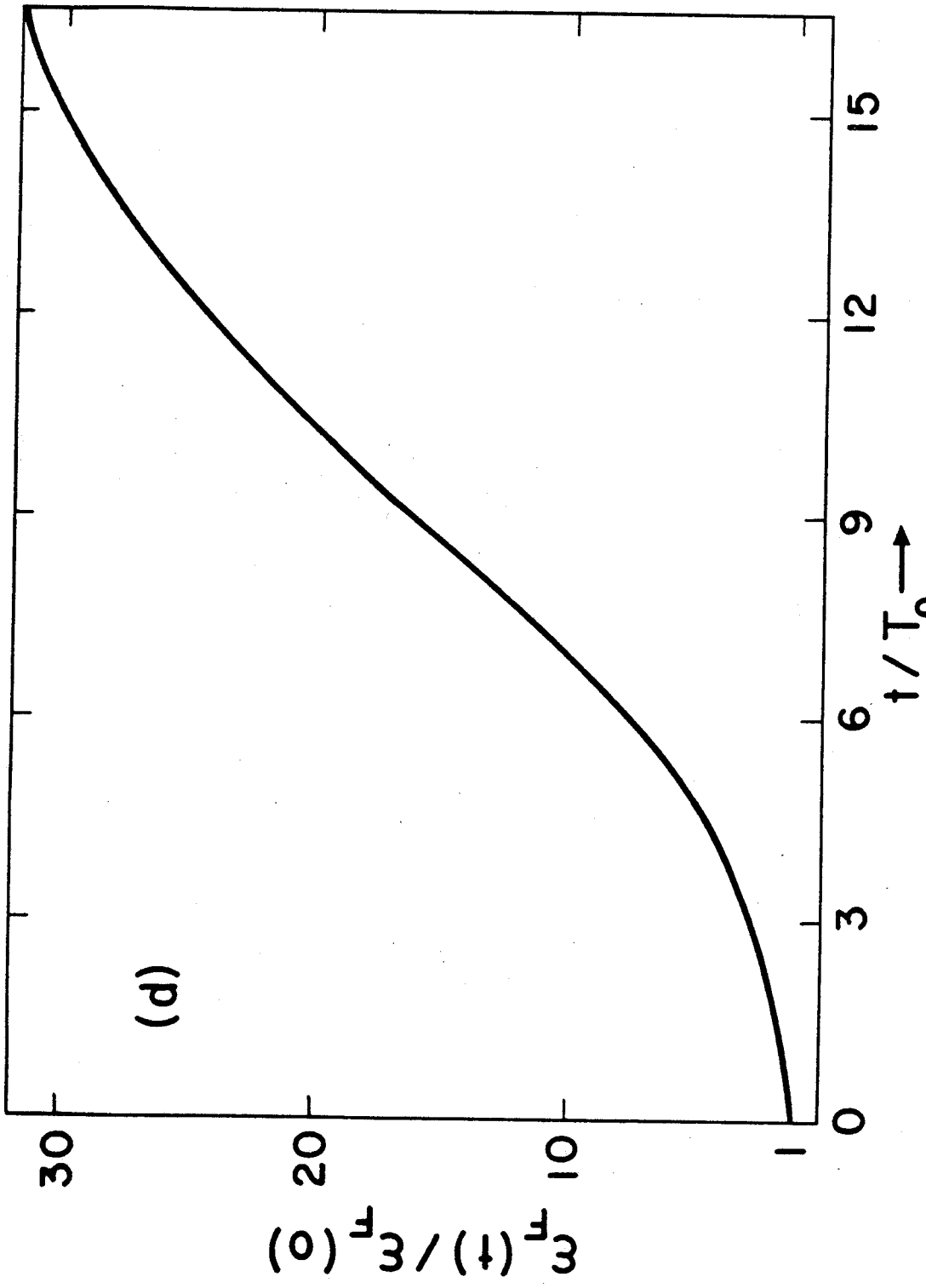

Fig. 6(d)

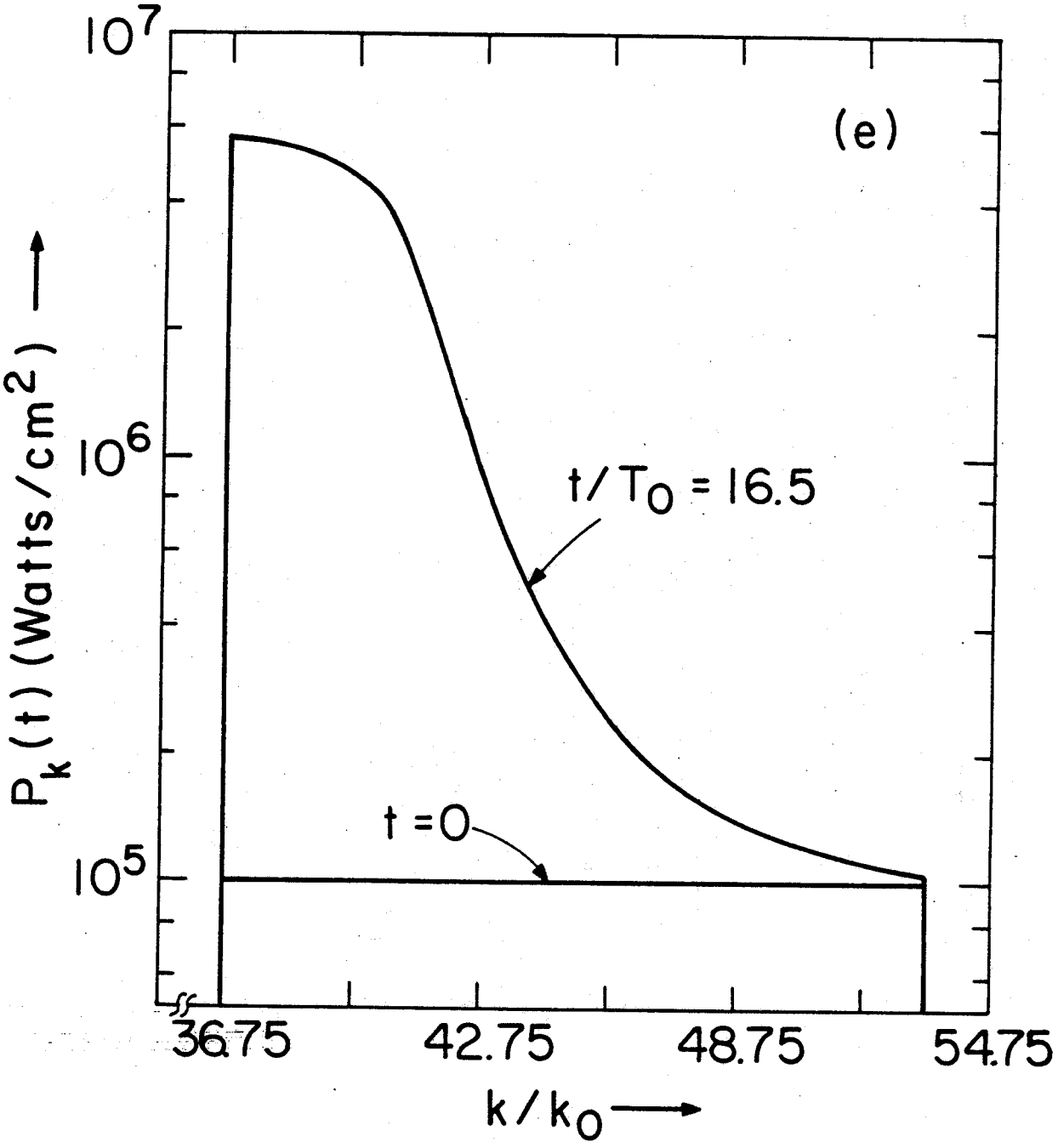

Fig. 6(e)

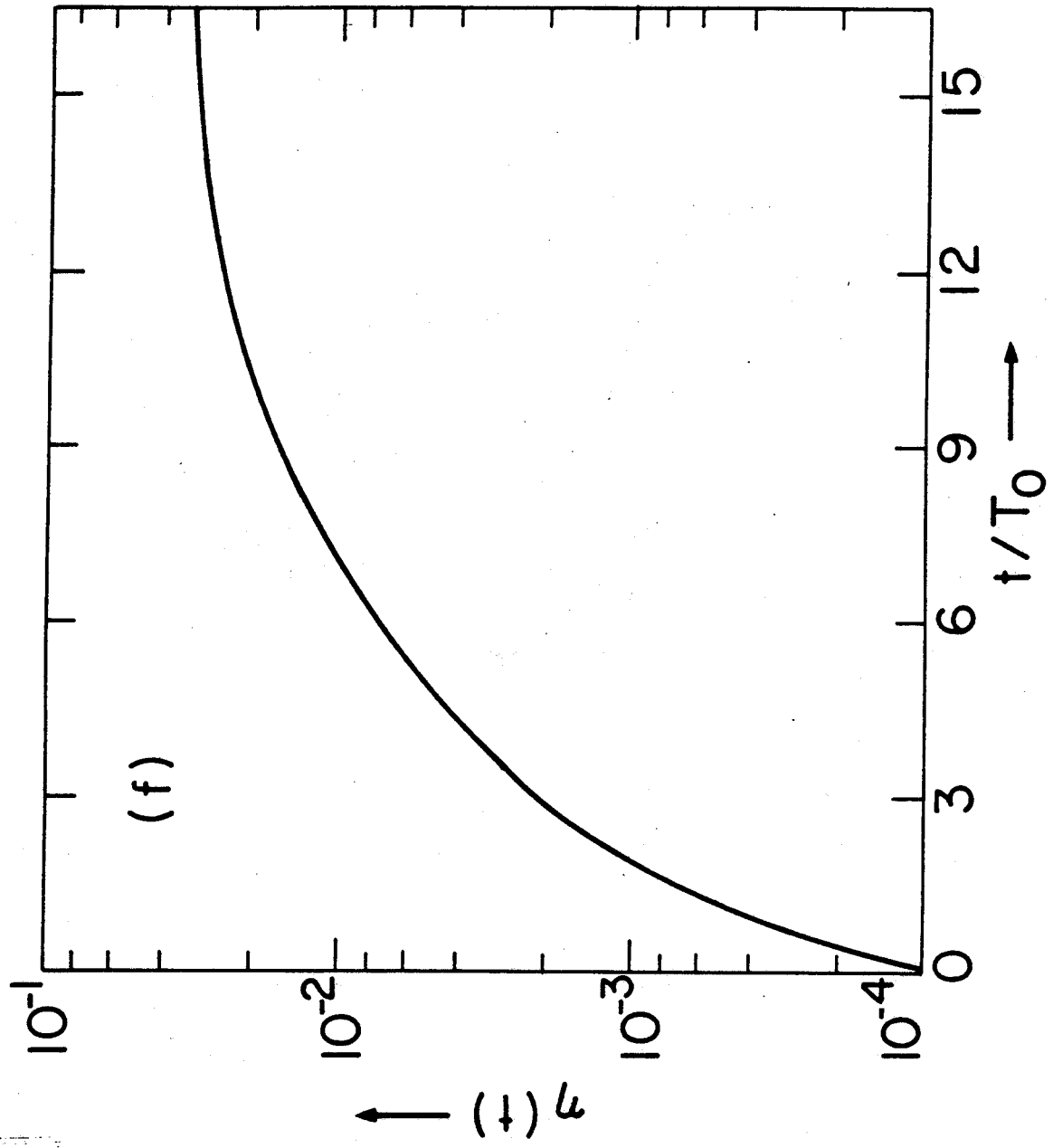

Fig. 6(f)

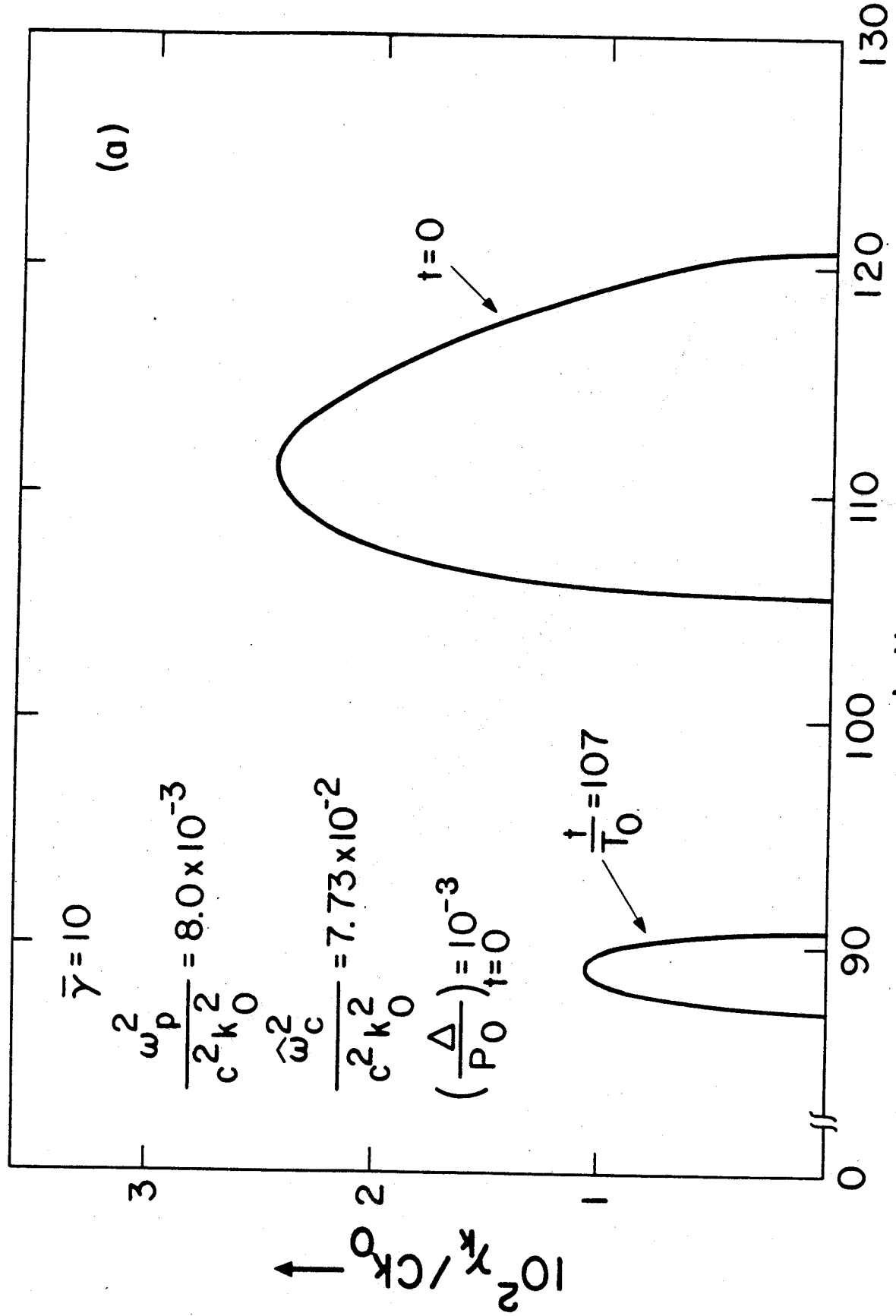
(a)
t=0
$\frac{t}{T_0}$=107
$\bar{\gamma}$=10
$\frac{\omega_p^2}{c^2k_0^2}$ = 8.0x10^{-3}
$\frac{\hat{\omega}_c^2}{c^2k_0^2}$ = 7.73x10^{-2}
$\left(\frac{\Delta}{P_0}\right)_{t=0}$ = 10^{-3}
10^2 γ_k/ck$_0$
k/k$_0$
0
90
100
110
120
130
1
2
3

Fig 7(a)

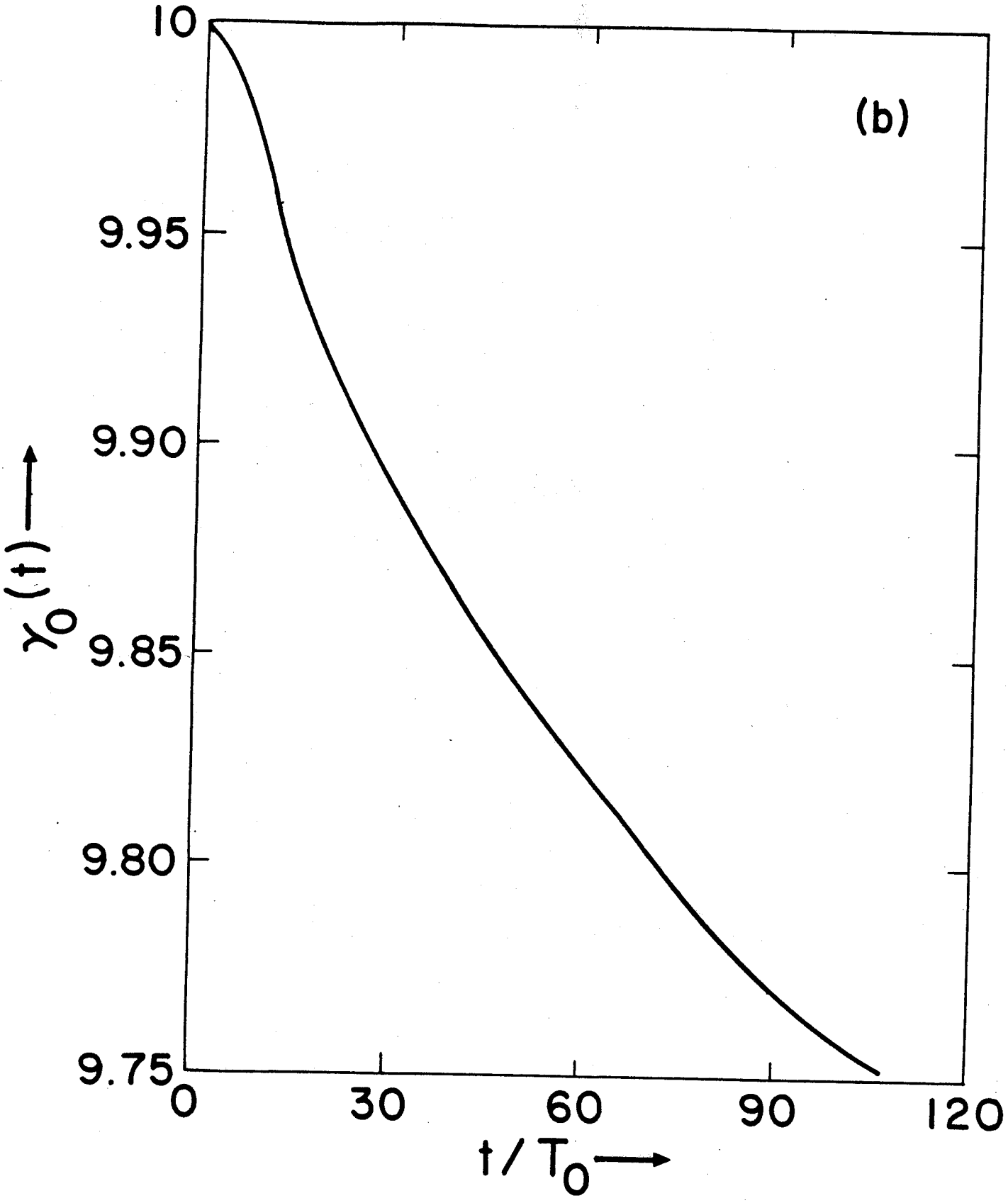

Fig. 7(b)

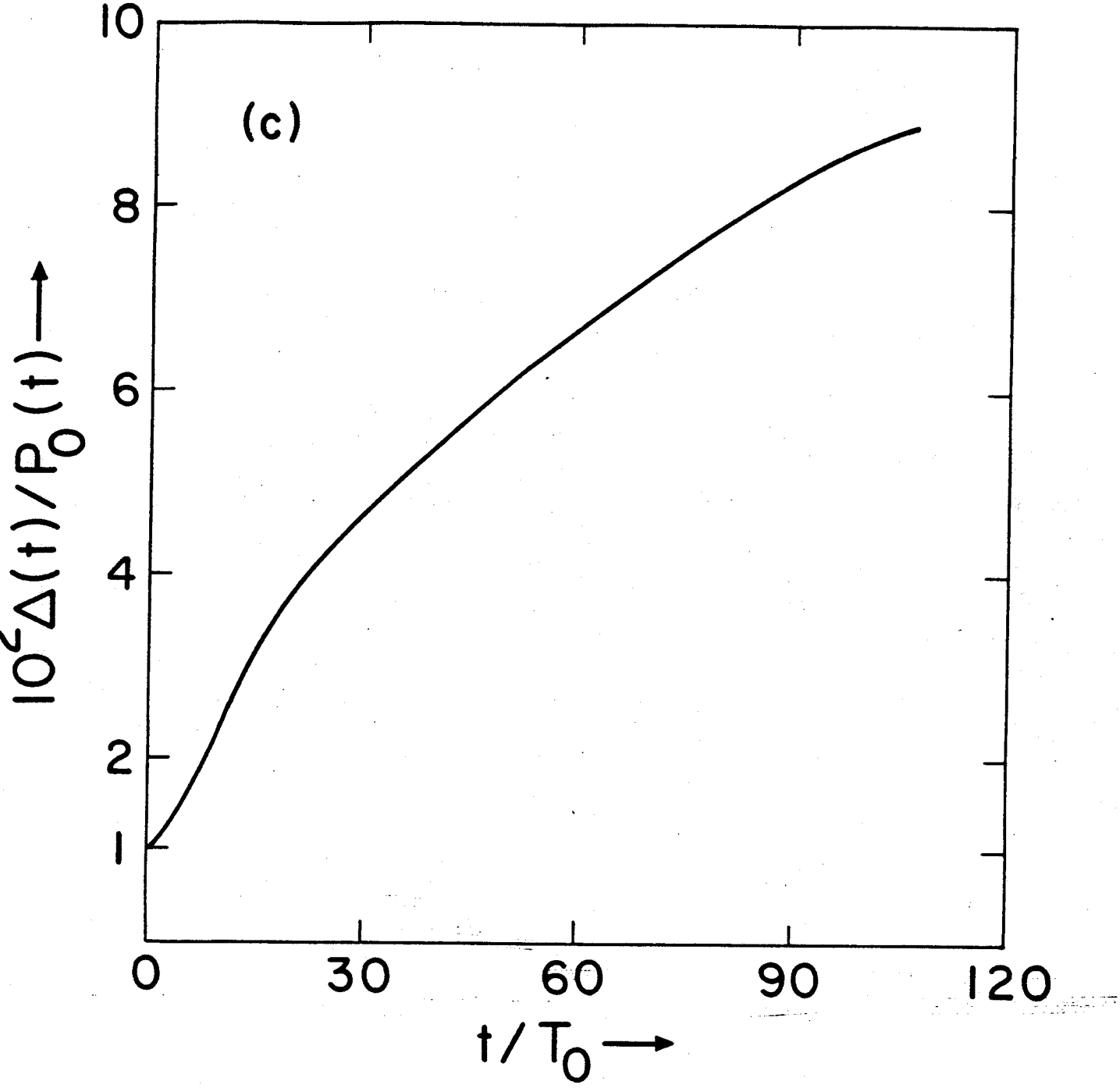

Fig. 7(c)

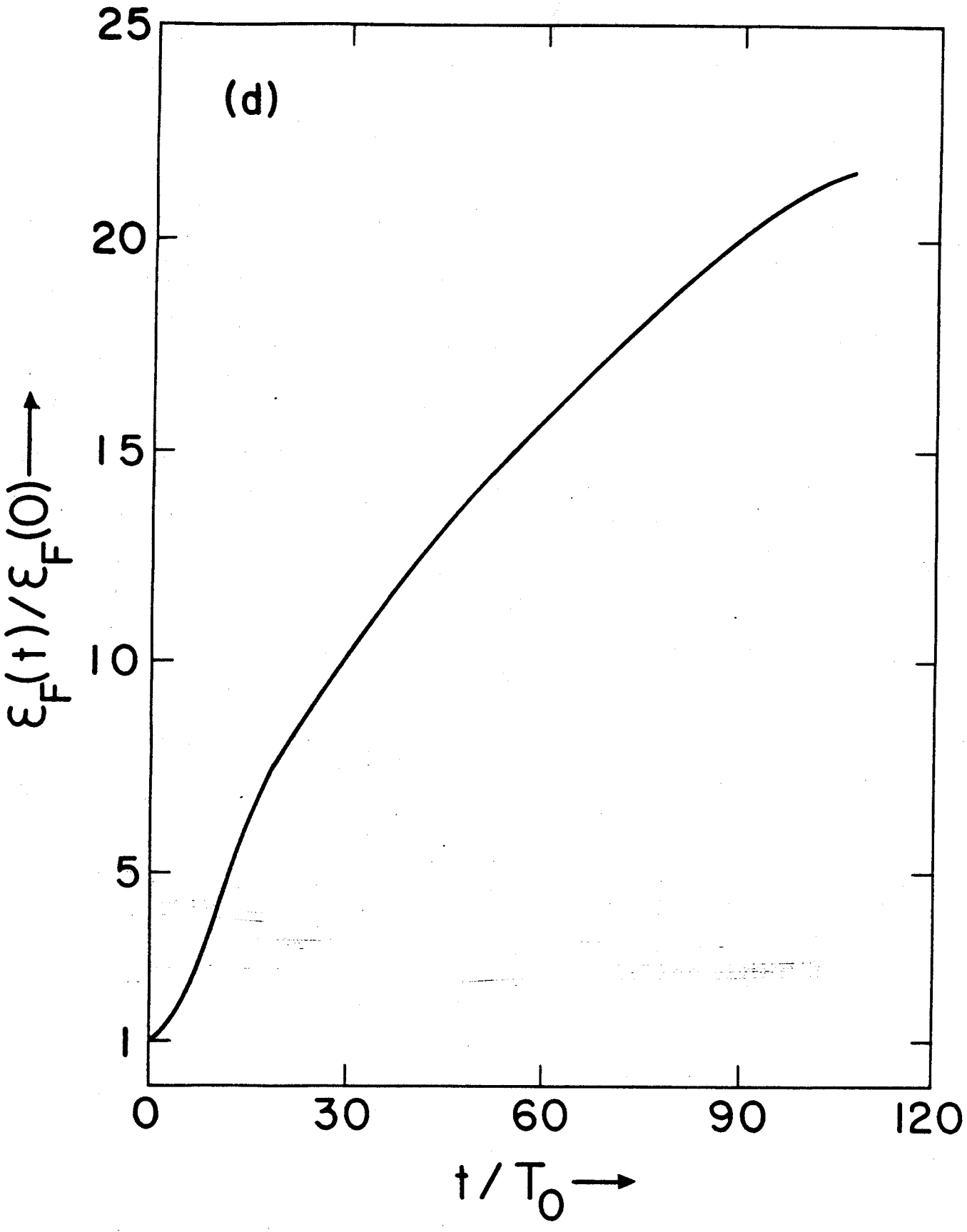

Fig. 7(d)

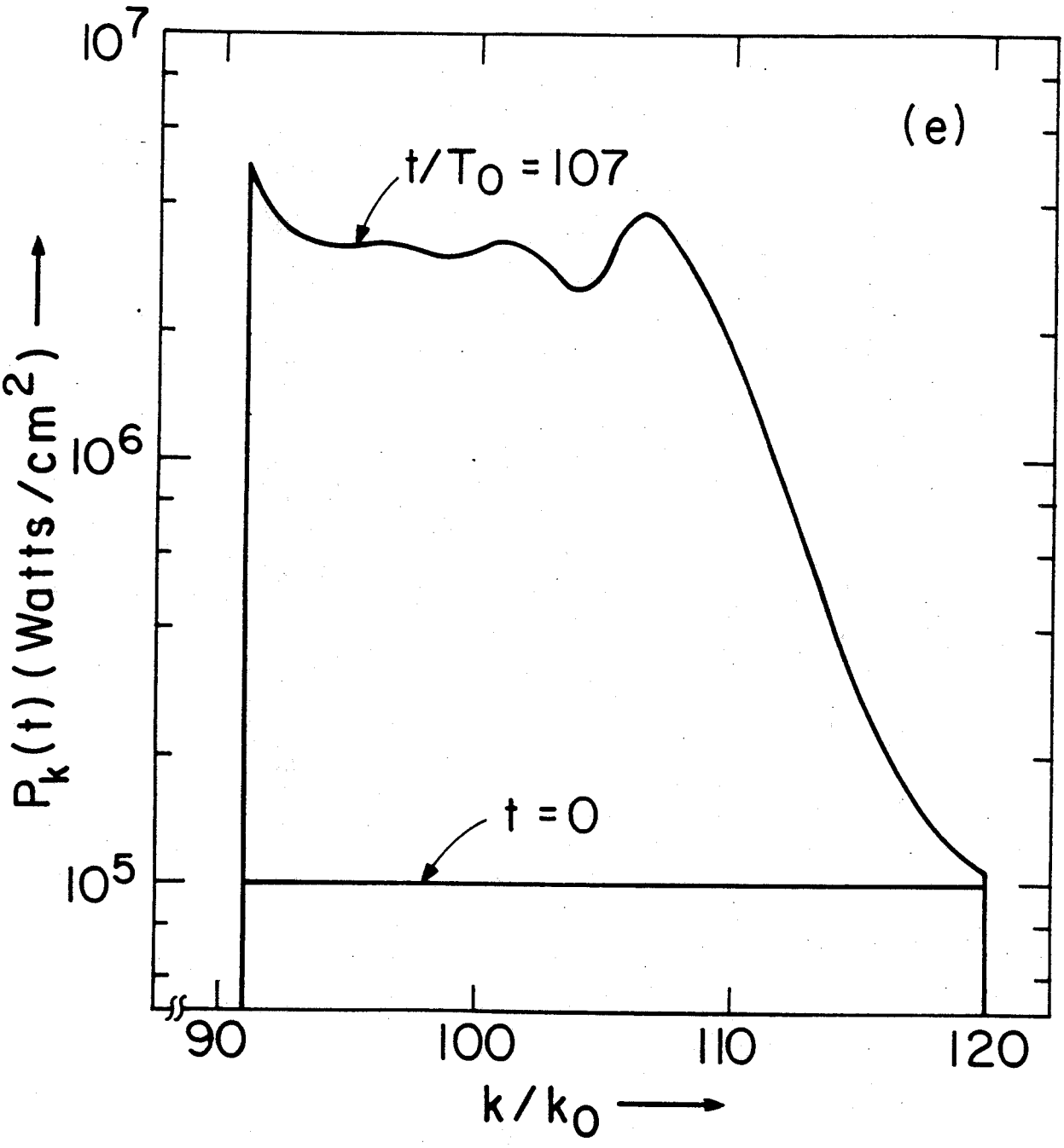

Fig. 7(e)

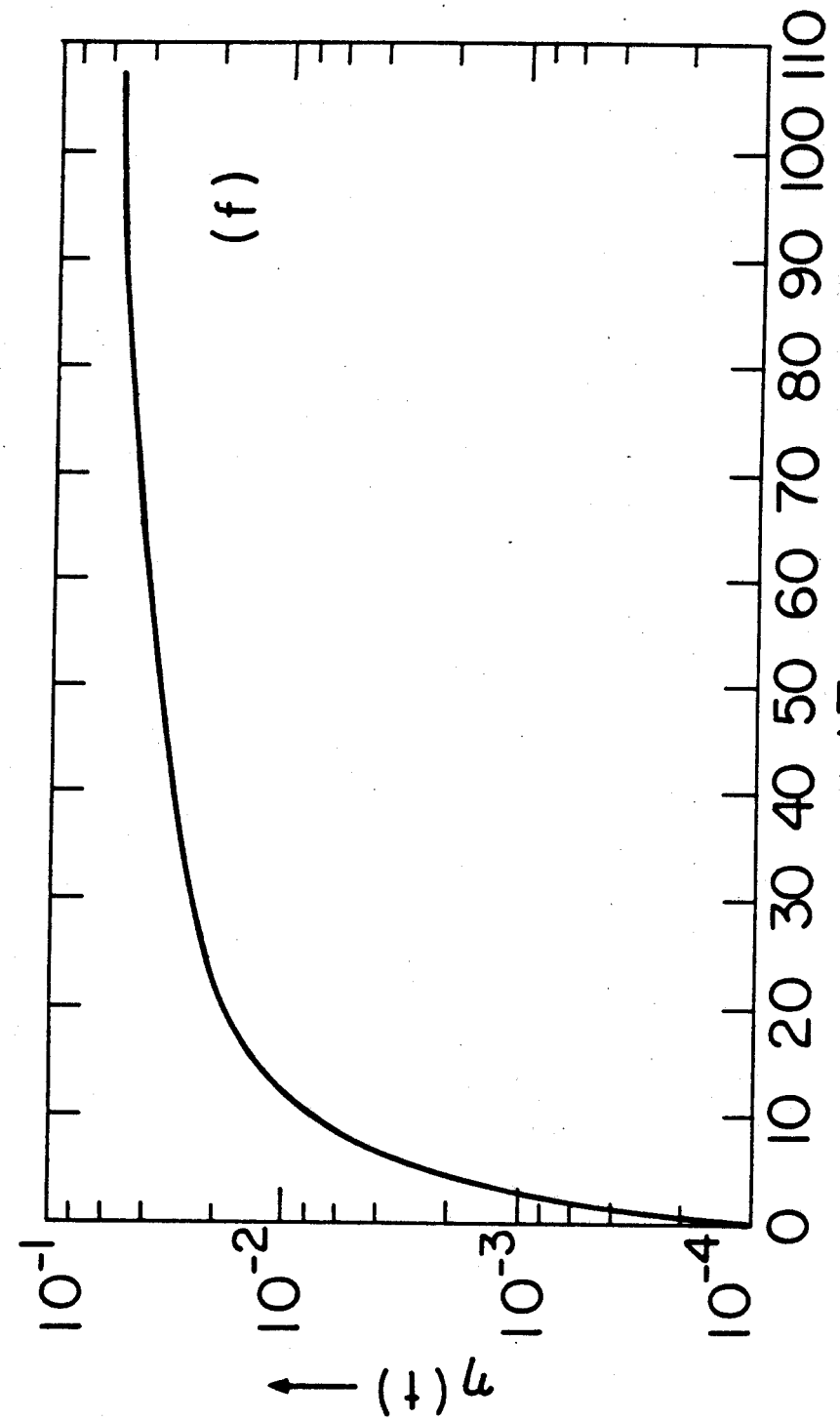

Fig. 7(f)

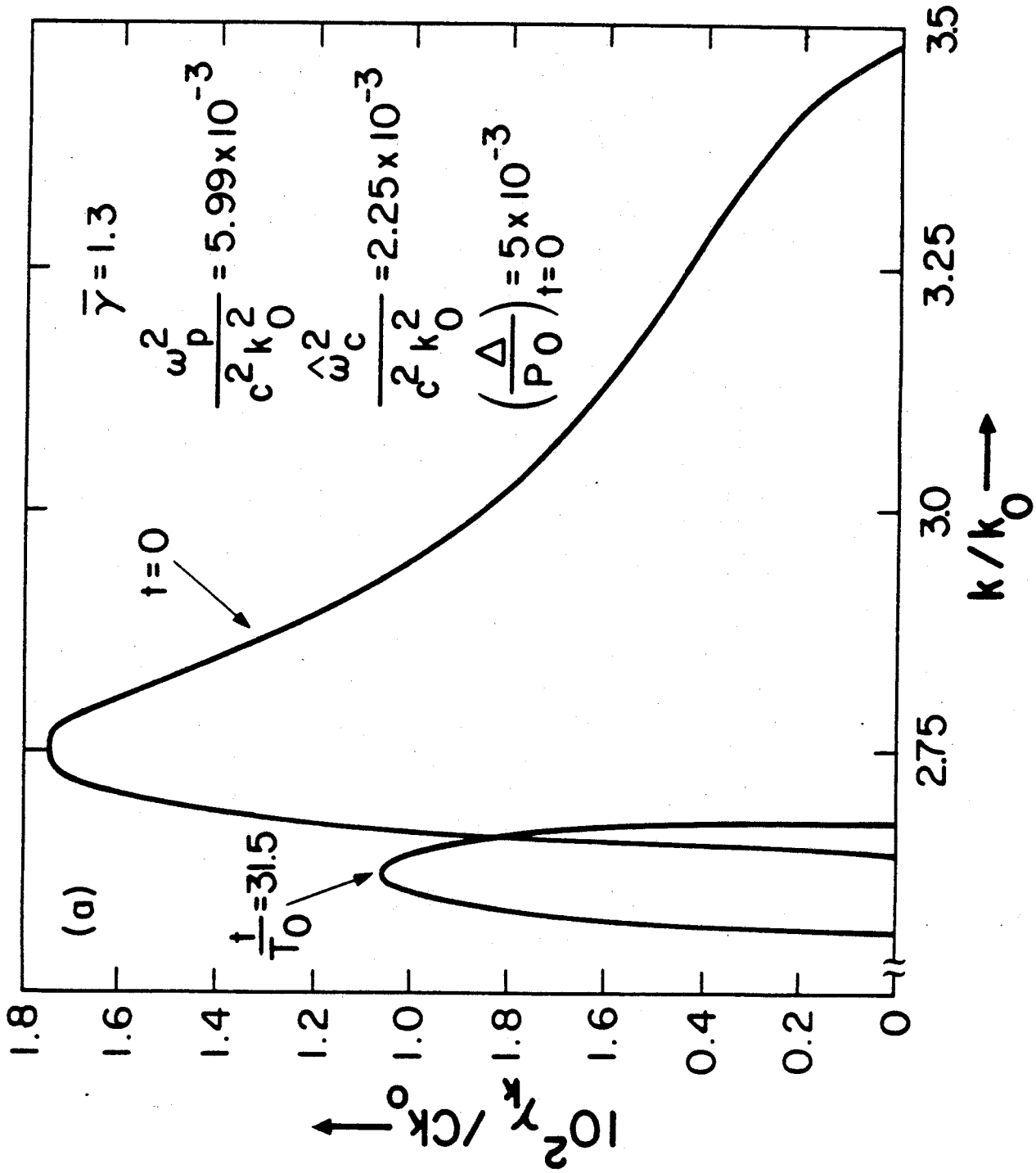
$10^2\gamma_k/ck_o$
1.8
1.6
1.4
1.2
1.0
1.8
1.6
0.4
0.2
0
2.75
3.0
3.25
3.5
k/k_o
(a)
$\frac{t}{T_o}=31.5$
t=0
$\bar{\gamma}=1.3$
$\frac{\omega_p^2}{c^2k_o^2}=5.99\times10^{-3}$
$\frac{\hat{\omega}_c^2}{c^2k_o^2}=2.25\times10^{-3}$
$\left(\frac{\Delta}{P_o}\right)_{t=0}=5\times10^{-3}$

Fig. 8(a)

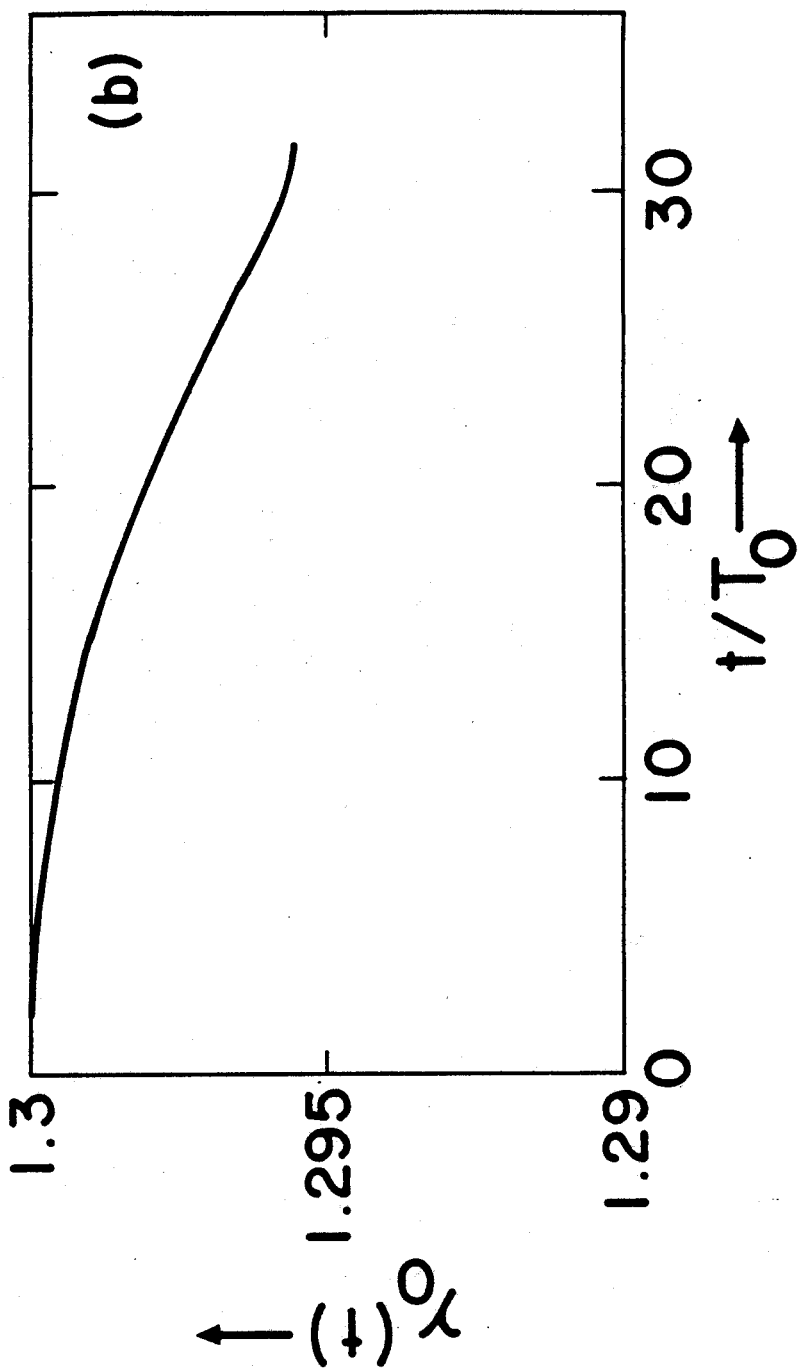

Fig. 8(b)

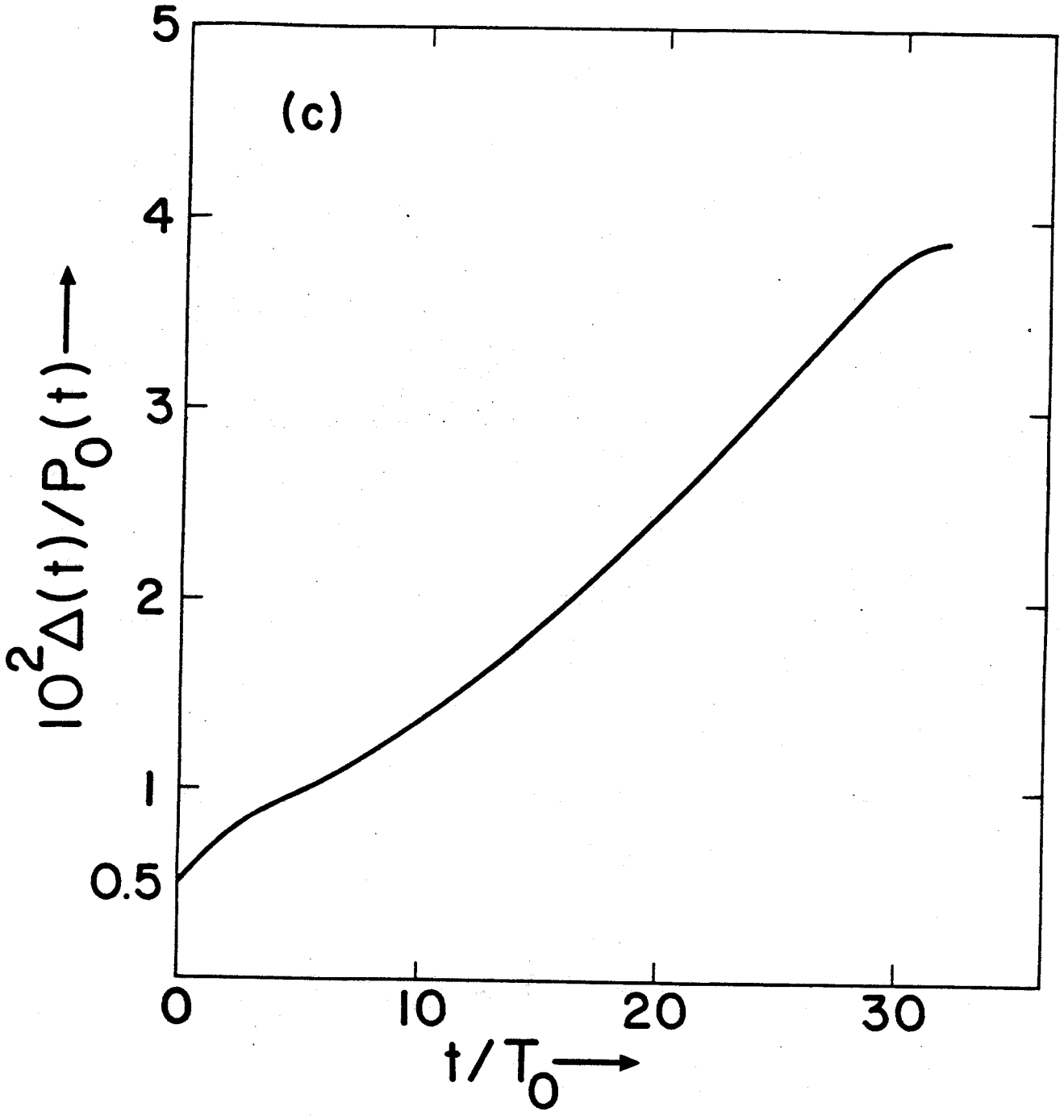

Fig. 8(c)

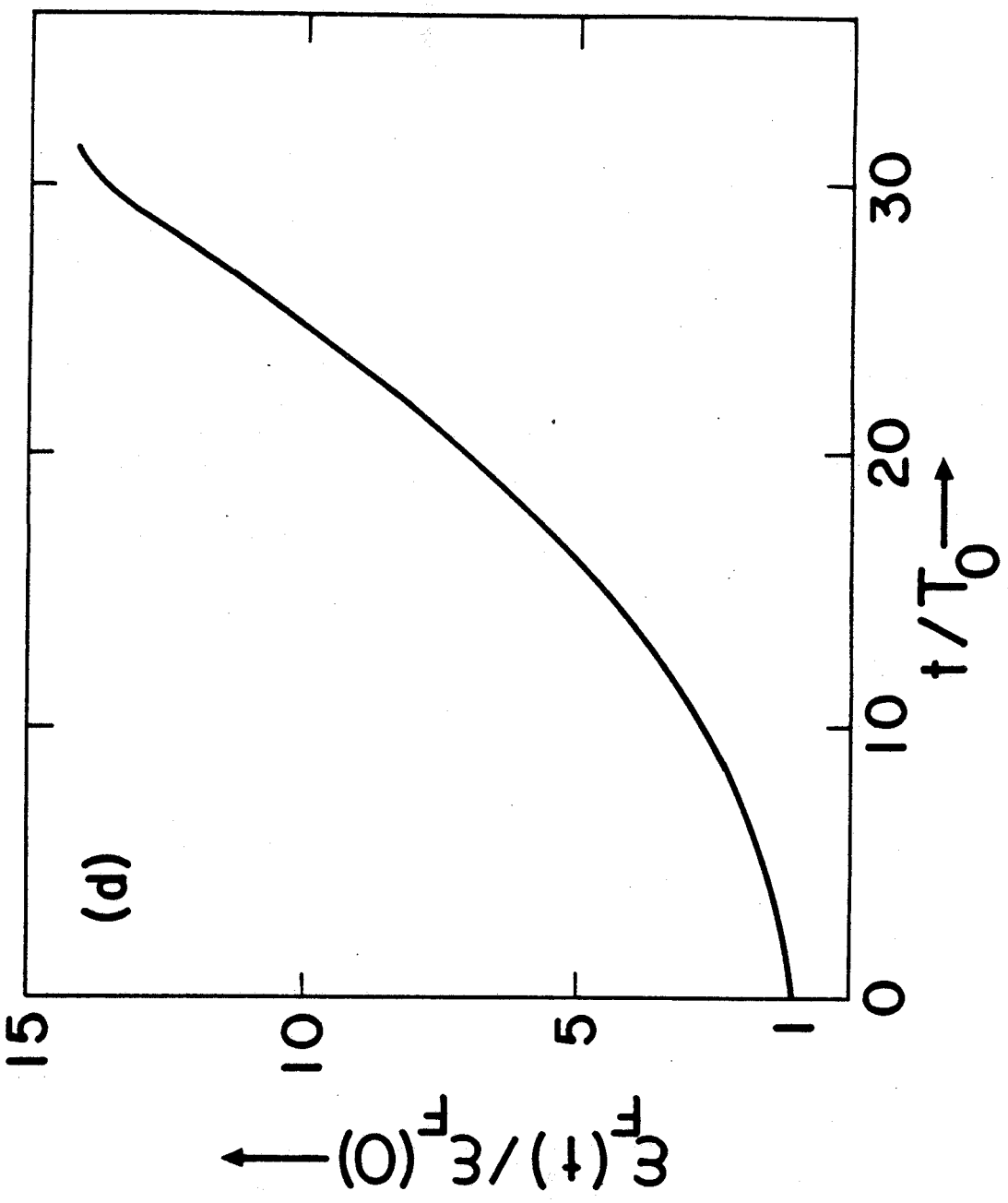

Fig. 8(d)

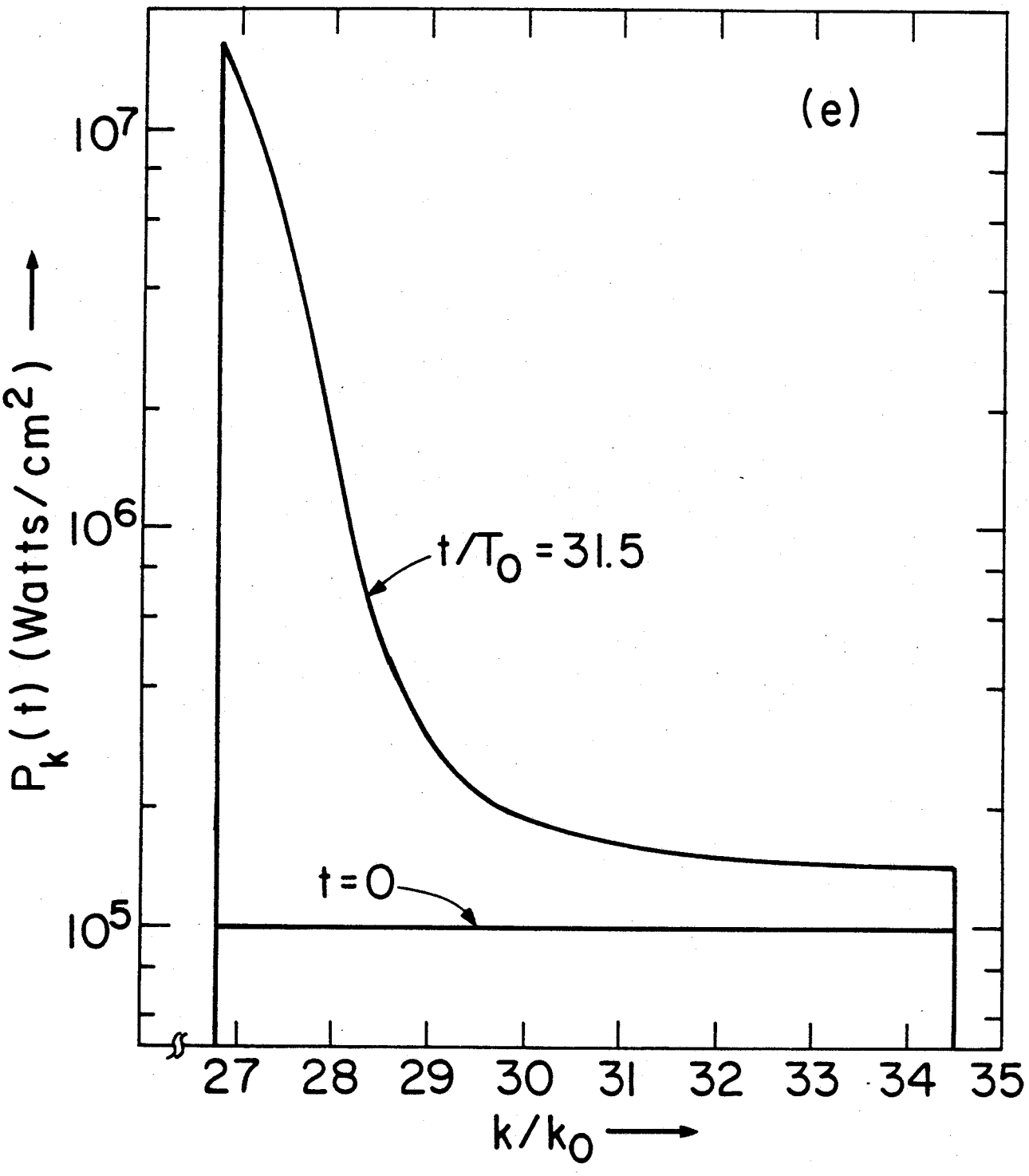
(e)
10^7
10^6
10^5
$P_k(t)$ (Watts/cm^2) ⟶
$t/T_0 = 31.5$
$t = 0$
27 28 29 30 31 32 33 34 35
k/k_0 ⟶

Fig. 8(e)

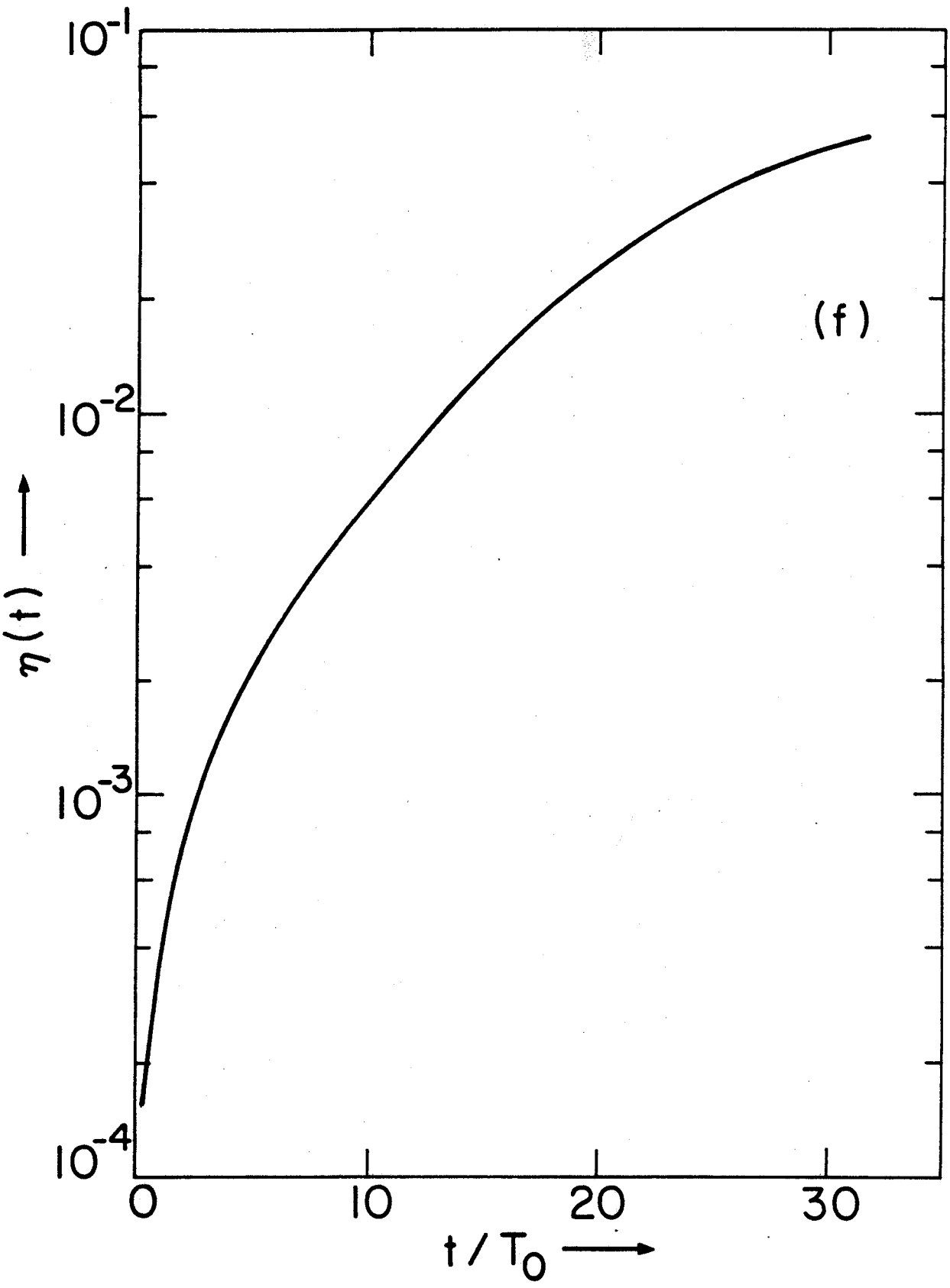

Fig. 8(f)